JOINT INSTITUTE FOR AERONAUTICS AND ACOUSTICS

National Aeronautics and Space Administration
Ames Research Center

NASA-CR-166174
19810013342

Stanford University

JIAA TR - 27

TRANSMITTED SOUND FIELD DUE TO AN IMPULSIVE LINE ACOUSTIC SOURCE BOUNDED BY A PLATE FOLLOWED BY A VORTEX SHEET

Toshiki Miura and C.C. Chao

STANFORD UNIVERSITY
Department of Aeronautics and Astronautics
Stanford, California 94305

JANUARY 1980

JIAA TR - 27

TRANSMITTED SOUND FIELD DUE TO AN IMPULSIVE LINE ACOUSTIC SOURCE BOUNDED BY A PLATE FOLLOWED BY A VORTEX SHEET

TOSHIKI MIURA AND C. C. CHAO

JANUARY 1980

The work here presented has been supported by the National Aeronautics and Space Administration under Contract NASA 2007.

ACKNOWLEDGMENTS

The authors wish to express their appreciation to Professor and Director of the Institute, K. Karamcheti, for his continued support and interest in all phases of this investigation, to Professor Harold Levine for his advice and valuable suggestions, and to Professor David G. Crighton for his helpful comments and discussions. The junior author wishes to acknowledge his appreciation for the financial support given to him by Mitsui Engineering and Shipbuilding Co., Ltd., Japan, during the period of his stay at Stanford University.

ABSTRACT

The propagation of sound due to a line acoustic source in the moving stream across a semi-infinite vortex sheet which trails from a rigid plate is examined in a linear theory for the subsonic case. A solution for the transmitted sound field is obtained with the aid of multiple integral transforms and the Wiener-Hopf technique for both the steady-state (time-harmonic) and initial-value (impulsive source) situations. The contour of inverse transform and hence the decomposition of the functions are determined through causality and radiation conditions. The solution obtained satisfies causality and the full Kutta conditions. The transmitted sound field is composed of two waves in both the steady-state and initial-value problems. One is the wave scattered from the edge of the plate which is associated with the bow wave and the instability wave. These bow waves and instability waves exist in the downstream sectors. The other is the wave transmitted through the vortex sheet which is also associated with the instability wave. This instability wave exists in a downstream sector, but if the line source is close to the rigid plate it is blocked by the plate and does not appear. The transmitted sound field can be divided into three regions. The first one is the region where the incident wave is shaded by the plate and only the wave scattered from the plate edge exists. In the second region there exist the waves transmitted through the

vortex sheet in addition to the scattered waves from the edge of the plate. The third region is the transition region between the two regions just described. In this region the waves transmitted through the vortex sheet can be heard partially depending on its wave number. The asymptotic nature of this region is the same as that of the second region.

TABLE OF CONTENTS

CHAPTER 1

INTRODUCTION

The influence of a moving stream on the propagation of sound is a problem of some practical importance and has attracted a number of investigations in recent years. For the sake of analytical simplicity, most theoretical investigations related to this problem have been confined to the model study of two infinite two-dimensional, inviscid fluid half-spaces in relative motion separated by a plane vortex sheet. Sound waves emitted from impulsive (harmonic) line or point sources will impinge on the vortex sheet and be reflected and transmitted to the two half-spaces as reflected and transmitted sound fields.

For linearized theory, multiple-Fourier transform techniques are most conveniently used to obtain the analytical solutions for these sound fields. While it is almost trivial to find the transformed solutions, the complexities of inverse transforms present much difficulty in finding a solution in a form most suitable for practical applications.

Jones and Morgan and their associates [1-5] in a series of papers investigated the problem of line and point sources. As they carried out inverse transform with respect to wave number first along the real axis, their solutions did not satisfy causality. To satisfy causality, they had to add the homogeneous solution which corresponds to instability waves. Chao [6] has indicated that if the inverse transform is carried out with respect to frequency first, the proper deformation of contour

which brings the causal solution is obvious and the instability waves are automatically included in the solution obtained.

In the real world a vortex sheet between two fluids in relative motion can only exist downstream of a plate which separates them. The problem becomes a mixed boundary value problem and the Wiener-Hopf technique [7-8] has to be used to find the transformed solution. Orszag and Crow [9] have investigated this problem in which there are no external sound sources and the flow is incompressible. Crighton [10] has extended their analysis to compressible subsonic flow. Morgan [11] and Crighton and Leppington [12] have investigated the reflected sound field produced by a line source near a semi-infinite vortex sheet which trails from a rigid plate where a line source is situated in the still fluid.

All of these problems require the decomposition of a known function into plus and minus functions which are analytic in the lower and upper wave number plane, respectively. However, due to the fact that there are poles whose location is frequency-dependent in such a way that it will move from lower half-plane to upper half wave number plane according to the value of frequency, the determination of a common region of analyticity and hence the contour of the inverse transform becomes a rather complicated matter and consequently requires additional assumptions to ascertain the desired contour of the inverse transform. Morgan has enforced the condition that the slope as well as the displacement of the vortex sheet are assumed to be zero at the plate edge (full Kutta condition).

Crighton and Leppington have decomposed the function by assuming a large imaginary part for the frequency. They both have shown that their assumptions require a deformation of the contour of the inverse transform and satisfy the criterion for causality established by Jones and Morgan [13]. This criterion requires the analyticity of the solution in the upper half frequency plane for causality and has been used successfully by Morgan [14] and Munt [15] in their analysis of the cylindrical vortex sheet problem.

In Chapter 4 it is shown that the deformation of the contour, and hence the common region of analycity can be determined through causality, exponential decay of the functions, and radiation condition. In all three of these approaches, the decomposition of the function is unique.

In Chapter 5 we determine the value of the entire function, assuming the edge condition that the component of the disturbed velocity in the stream direction is finite at the edge of the plate. This assumption requires that the full Kutta condition be satisfied as a result. Howe [16] has found that for a very low Mach number flow case, the satisfaction of the Kutta condition requires that external forces be present in the vicinity of the plate edge. Similar situations certainly would occur for the present problem. The existence of this external force probably can be traced to the viscous effect which should not be neglected due to the large velocity gradient in the vicinity of the plate edge. A detailed study of viscous mixing at a trailing edge by Daniels [17] suggests that the full Kutta condition is the logical

condition to apply at the plate edge. A further justification of the Kutta condition may be found in the experimental work by Bechert and Pfizenmaier [18]. Their work suggests that the full Kutta condition is the correct condition to apply if the shear layer is thin, which is the case in our problem.

In Chapter 6 the solution is compared with that of the Sommerfeld half-plane diffraction problem (without the flow). It is found that the existence of the flow smooths the edge behavior of the solution.

In Chapter 7 the steady-state solution is calculated. The transmitted sound field can be divided into three regions depending on how the waves transmitted through the vortex sheet are shaded by the rigid plate. In Region 1, the incident wave is shaded completely by the plate and only the waves scattered from the plate edge exist. In Region 2 the waves transmitted through the vortex sheet exist in addition to the edge scattered waves. Region 3 is the transition region between the two where the part of the waves transmitted through the vortex sheet exist depending on its wave number. The existence of Region 3 is the direct conclusion of the fact that the line source and observer are located in the different mediums. It is expected that a similar situation will occur if the speed of sound is different between the two mediums even though the velocities of the flows in the two mediums are the same.

In Chapter 8 the asymptotic evaluation of the transmitted sound field is carried out as far as possible. In the case where the line

source is situated close to the plate edge in comparison to the observer, the asymptotic nature of Region 3 is similar to that of Region 2, and in the far field the boundary between Regions 2 and 3 vanishes.

In Chapter 9, the solution for the initial value problem is calculated. The wave fronts of the diffracted waves are obtained explicitly.

CHAPTER 2

FORMULATION OF THE PROBLEM

Consider the problem in which a moving fluid in the half-space $y < 0$ is separated by a rigid plate and a vortex sheet from a still medium in $y > 0$. The rigid plate occupies the half-plane $y = 0$, $x < 0$, the vortex sheet occupies $y = 0$, $x > 0$ in a Cartesian coordinate system and it is assumed that the flow is in the direction of increasing x. A line source of unit strength is situated in parallel to the x-axis through (x_o, y_o) in the moving medium, so that $y_o < 0$ (Figure 2-1). For the sake of simplicity, the sound speed and density are assumed to be the same in both fluids. Because of the symmetry of the problem all quantities are independent of z.

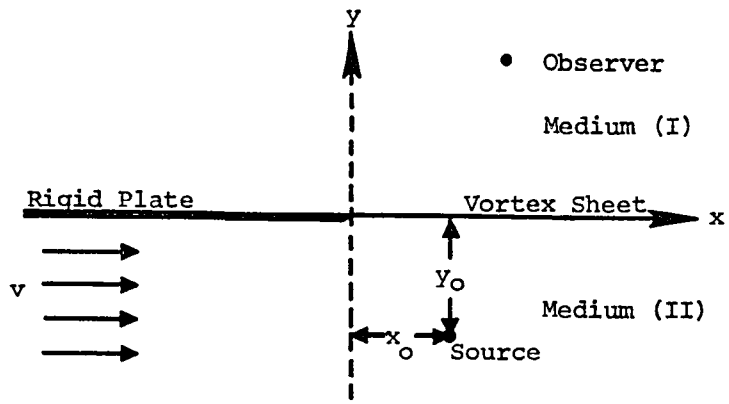

Figure 2-1 Sketch of the Model Geometry

Let ϕ_1 and ϕ_2 denote the velocity potentials of the small disturbed motions in the two fluid spaces. Due to the excitation of the line source, the governing differential equations for ϕ_1 and ϕ_2 are:

$$\left.\begin{aligned} &\left(\frac{\partial}{\partial t} + V\frac{\partial}{\partial x}\right)^2\phi_2 - a^2\nabla^2\phi_2 = \delta(x-x_o)\,\delta(y-y_o)\delta(t) \qquad (y<0)\\ &\frac{\partial^2\phi_1}{\partial t^2} - a^2\nabla^2\phi_1 = 0 \qquad\qquad\qquad\qquad\qquad\quad (y>0) \end{aligned}\right\} \tag{2-1}$$

where a is the speed of the sound and V is the velocity of the moving flow.

Define the Fourier transform of ϕ_i as:

$$\bar{\bar{\phi}}_1(k,y,\omega) = \frac{1}{4\pi^2}\int_{-\infty}^{\infty}\int_{-\infty}^{\infty}\phi_1(x,y,t)e^{-i(kx-\omega t)}dxdt\ . \tag{2-2}$$

Then Eqs. (2-1) reduce to the form:

$$\left.\begin{aligned} &\frac{\partial^2\bar{\bar{\phi}}_2}{\partial y^2} + \gamma_2^2\bar{\bar{\phi}}_2 = \frac{-\delta(y-y_o)e^{-ikx_o}}{4\pi^2a^2}\\ &\frac{\partial^2\bar{\bar{\phi}}_1}{\partial y^2} + \gamma_1^2\bar{\bar{\phi}}_1 = 0 \end{aligned}\right\} \tag{2-3}$$

where

$$\gamma_2^2 = \left(\frac{\omega}{a} - Mk\right)^2 - k^2$$

$$\gamma_1^2 = \left(\frac{\omega}{a}\right)^2 - k^2$$

and $M = \frac{V}{a}$ is the Mach number of the lower medium. Let $y = h(x,t)$ indicate the equation of the vortex sheet. The boundary conditions on the vortex sheet are the continuity of pressure, giving

$$\left(\frac{\partial}{\partial t} + V\frac{\partial}{\partial x}\right)\phi_2 = \frac{\partial \phi_1}{\partial t} , \tag{2-4}$$

and the kinematic condition of the continuity of particle displacement which implies

$$\left\{\frac{\partial}{\partial t} + \left(V + \frac{\partial \phi_2}{\partial x}\right)\frac{\partial}{\partial x} + \frac{\partial \phi_2}{\partial y}\frac{\partial}{\partial y}\right\} H(x,y,t) = 0 , \tag{2-5}$$

where $H(x,y,t) = y - h(x,t)$. Linearizing the equation, we have

$$\left(\frac{\partial}{\partial t} + V\frac{\partial}{\partial x} + \frac{\partial \phi_2}{\partial y}\frac{\partial}{\partial y}\right)(y-h) = 0$$

and

$$-\frac{\partial h}{\partial t} - V\frac{\partial h}{\partial x} + \frac{\partial \phi_2}{\partial y}\frac{\partial y}{\partial y} = 0 .$$

We get:

$$\frac{\partial \phi_2}{\partial y} = \frac{\partial h}{\partial t} + V\frac{\partial h}{\partial x} . \tag{2-5a}$$

Similarly, for medium (I)

$$\frac{\partial \phi_1}{\partial y} = \frac{\partial h}{\partial t} . \tag{2-5b}$$

The boundary condition for $x < 0$ is the vanishing of the normal velocity on the splitter plate which implies

$$\frac{\partial \phi_1}{\partial y} = \frac{\partial \phi_2}{\partial y} = 0, \quad h = 0 \ . \tag{2-6}$$

Define the half-range Fourier transforms of ϕ_1 and h as:

$$\overline{\overline{\phi}}_{i+}(k,y,\omega) = \frac{1}{4\pi^2} \int_{-\infty}^{\infty} \int_{0}^{\infty} \phi_1(x,y,t) e^{-i(kx-\omega t)} dxdt \tag{2-7a}$$

$$\overline{\overline{h}}_{+}(k,\omega) = \frac{1}{4\pi^2} \int_{-\infty}^{\infty} \int_{0}^{\infty} h(x,t) e^{-i(kx-\omega t)} dxdt \tag{2-7b}$$

$$\overline{\overline{\phi}}_{i-}(k,y,\omega) = \frac{1}{4\pi^2} \int_{-\infty}^{\infty} \int_{-\infty}^{0} \phi_i(x,y,t) e^{-1(kx-\omega t)} dxdt \tag{2-7c}$$

$$\overline{\overline{h}}_{-}(k,\omega) = \frac{1}{4\pi^2} \int_{-\infty}^{\infty} \int_{-\infty}^{0} h(x,t) e^{-1(kx-\omega t)} dxdt \ . \tag{2-7d}$$

Equations (2-4), (2-5a), (2-5b), and (2-6) reduce to the form

$$- 1\omega \overline{\overline{\phi}}_{2+} + \frac{V}{2\pi} \int_{0}^{\infty} \frac{\partial \overline{\phi}_2}{\partial x}(x,y,\omega) \, e^{-1kx} dx = -1\omega \overline{\overline{\phi}}_{1+}$$

$$\overline{\overline{\phi}}_{2+} + \frac{V1}{2\pi\omega} \left[\overline{\phi}_2 e^{-ikx} \Big|_{0}^{\infty} + ik \int_{0}^{\infty} \overline{\phi}_2 e^{-1kx} dx \right] = \overline{\overline{\phi}}_{1+} \ ,$$

$$\alpha \overline{\overline{\phi}}_{2+} + L_1 = \overline{\overline{\phi}}_{1+} \ , \tag{2-8}$$

where

$$\alpha = 1 - \frac{Vk}{\omega}$$

$$L_1 = - \frac{Vi}{2\pi\omega} \bar{\phi}_2(x,y,\omega) \Big|_{x,y=0}$$

$$\frac{\partial \bar{\bar{\phi}}_{2+}}{\partial y} = - i\omega \bar{\bar{h}}_+ + \frac{V}{2\pi} \int_0^\infty \frac{\partial \bar{h}(x,y,\omega)}{\partial x} e^{-ikx} dx$$

$$= - \imath\omega \bar{\bar{h}}_+ + \frac{V}{2\pi} \left[\bar{h}\, e^{-ikx} \Big|_0^\infty + \imath k \int_0^\infty \bar{h}\, e^{-ikx} dx \right]$$

$$= - i\omega\alpha \bar{\bar{h}}_+ . \qquad (2\text{-}9)$$

Here, we use the condition $h\big|_{x=0} = \bar{h}\big|_{x=0} = 0$, because at the edge of the plate, the vortex sheet must attach to the plate. Similarly,

$$\frac{\partial \bar{\bar{\phi}}_{1+}}{\partial y} = - \imath\omega \bar{\bar{h}}_+ \qquad (2\text{-}10)$$

and

$$\frac{\partial \bar{\bar{\phi}}_{1-}}{\partial y} = \frac{\partial \bar{\bar{\phi}}_{2-}}{\partial y} = 0 \qquad \bar{\bar{h}}_- = 0 . \qquad (2\text{-}11)$$

Solutions to the set of the ordinary differential Eq. (2-3) can be easily found as:

$$\left.\begin{aligned} \bar{\bar{\phi}}_1 &= A_1(k,\omega) e^{\imath\gamma_1 y} + B_1(k,\omega) e^{-i\gamma_1 y} \\ \bar{\bar{\phi}}_2 &= A_2(k,\omega) e^{-\imath\gamma_2 y} + B_2(k,\omega) e^{i\gamma_2 y} - \frac{e^{-ikx_o}}{4\pi^2 a^2 \gamma_2} \sin\left[\gamma_2 (y-y_o)\right] H(y-y_o) \end{aligned}\right\} \qquad (2\text{-}12)$$

where H( ) is the Heaviside step function. The sign conventions of γ_1 and γ_2 are chosen such that the signs of their imaginary part are always positive. Consequently, A_1 and A_2 terms of the solution are finite at infinity for all values of k and ω. B_1 and B_2 must be set to zero. Using the relation

$$\left.\frac{\partial \bar{\bar{\phi}}_1}{\partial y}\right|_{y=0} = i\gamma_1 \left.\bar{\bar{\phi}}_1\right|_{y=0}$$

$$\left.\frac{\partial \bar{\bar{\phi}}_2}{\partial y}\right|_{y=0} = -i\gamma_2 \left.\bar{\bar{\phi}}_2\right|_{y=0} - \frac{e^{-i(kx_o+\gamma_2 y_o)}}{4\pi^2 a^2}$$

$$\bar{\bar{\phi}}_1 = \bar{\bar{\phi}}_{i+} + \bar{\bar{\phi}}_{i-}$$

and the boundary conditions (2-9), (2-10), and (2-11), we obtain

$$\left.\bar{\bar{\phi}}_{1+}\right|_{y=0} = -\frac{\omega \bar{\bar{h}}_+}{\gamma_1} - \left.\bar{\bar{\phi}}_{1-}\right|_{y=0}$$

$$\left.\bar{\bar{\phi}}_{2+}\right|_{y=0} = \frac{\omega\alpha \bar{\bar{h}}_+}{\gamma_2} - \left.\bar{\bar{\phi}}_{2-}\right|_{y=0} + \frac{i\, e^{-i(kx_o+\gamma_2 y_o)}}{4\pi^2 a^2 \gamma_2} . \qquad (2\text{-}13)$$

Substituting these into Eq. (2-8) gives the Wiener-Hopf equation as:

$$\omega \bar{\bar{h}}_+ = K\left(\alpha \left.\bar{\bar{\phi}}_{2-}\right|_{y=0} - \left.\bar{\bar{\phi}}_{1-}\right|_{y=0} - L_1\right) - \frac{i\gamma_i \alpha\, e^{-i(kx_o+\gamma_2 y_o)}}{4\pi^2 a^2 (\gamma_2+\gamma_1\alpha^2)} \qquad (2\text{-}14)$$

where

$$K = \frac{\gamma_1\gamma_2}{\gamma_2+\gamma_1\alpha^2} .$$

If we can decompose K into plus and minus functions as:

$$K = \frac{K_-}{K_+} ,$$

we can rewrite the Wiener-Hopf equation as:

$$\omega\bar{\bar{h}}_+ K_+ = K_- \left(\alpha\bar{\bar{\phi}}_{2-}\Big|_{y=0} - \bar{\bar{\phi}}_{1-}\Big|_{y=0} - L_1 \right) - \frac{i\gamma_1 \alpha\, e^{-i(kx_o+\gamma_2 y_o)} K_+}{4\pi^2 a^2 (\gamma_2+\gamma_1\alpha^2)} . \qquad (2\text{-}15)$$

The last term of Eq. (2-15) can be decomposed into the sum of plus and minus functions as:

$$F = \frac{i\gamma_1 \alpha\, e^{-i(kx_o+\gamma_2 y_o)} K_+}{4\pi^2 a^2 (\gamma_2+\gamma_1\alpha^2)} = F_+ + F_- , \qquad (2\text{-}16)$$

where F_+, F_- are given as:

$$\left.\begin{aligned} F_+(k) &= \frac{-1}{2\pi i} \int_{C_+} \frac{F(\lambda)}{\lambda-k}\, d\lambda \\ F_-(k) &= \frac{1}{2\pi i} \int_{C_-} \frac{F(\lambda)}{\lambda-k}\, d\lambda . \end{aligned}\right\} \qquad (2\text{-}17)$$

The exponential decay of F(k) on the contour, since $\mathrm{Im}\gamma_2 > 0$, $y_o < 0$ ensures that these integrals exist and that $F_+(k) = 0(|k|^{-1})$, $F_-(k) = 0(|k|^{-1})$ as $|k| \to \infty$. The meaning of the plus and minus functions and the decomposition will be discussed in the next chapter.

Substituting Eq. (2-16) into Eq. (2-15) completes the decomposition, to give:

$$\bar{\bar{\omega h}}_+ K_+ + F_+ = K_- \left(\alpha \bar{\bar{\phi}}_{2-} \Big|_{y=0} - \bar{\bar{\phi}}_{1-} \Big|_{y=0} - L_1 \right) - F_1$$
$$= C(k) \ . \qquad (2\text{-}18)$$

The function C(k) defined by Eq. (2-18) is an entire function of k and must be a regular function of k in the whole k-plane. If C(k) is determined, $\bar{\bar{\omega h}}_+$ is given as:

$$\bar{\bar{\omega h}}_+ = \frac{1}{K_+} \left(C(k) - F_+ \right) \ . \qquad (2\text{-}19)$$

From Eq. (2-13)

$$A_1 = \frac{-C(k) + F_+}{\gamma_1 K_+}$$
$$A_2 = \frac{\alpha}{\gamma_2 K_+} \left[C(k) - F_+ \right] + \frac{i\, e^{-ikx_o}}{4\pi^2 a^2 \gamma_2} \cos \gamma_2 y_o \ . \qquad (2\text{-}20)$$

The solutions in the transformed region are determined.

CHAPTER 3

DECOMPOSITION OF THE FUNCTIONS

First, let us construct the branch cuts of γ_1 and γ_2 in the k-plane. To do this, the sign of $\mathrm{Im}\omega$ has to be investigated. One of the ways to determine the sign of $\mathrm{Im}\omega$ is to consider the wave equation with damping [8].

$$\nabla^2\phi - \frac{1}{a^2}\frac{\partial^2\phi}{\partial t^2} - \frac{\varepsilon}{a^2}\frac{\partial\phi}{\partial t} = 0 , \qquad \varepsilon > 0 . \tag{3-1}$$

Carrying out the Fourier transform, defined as:

$$\overline{\phi} = \frac{1}{2\pi}\int_{-\infty}^{\infty} \phi\, e^{i\omega t} dt , \tag{3-2}$$

Eq. (3-1) reduces to:

$$\nabla^2\overline{\phi} + \frac{\omega^2 + i\omega\varepsilon}{a^2}\overline{\phi} = 0 , \tag{3-3}$$

where ω is assumed to be real. Alternatively, assuming ω to be complex as $\omega = \omega_1 + i\omega_2$, where ω_1 and ω_2 are real and taking the wave equation which does not have damping,

$$\nabla^2\phi - \frac{1}{a^2}\frac{\partial^2\phi}{\partial t^2} = 0 . \tag{3-4}$$

Carrying out the Fourier transform, we obtain

$$\nabla^2\bar{\phi} + \frac{\omega_1^2 - \omega_2^2 + 2\omega_1\omega_2 i}{a^2}\bar{\phi} = 0 \ . \tag{3-5}$$

Comparing Eq. (3-3) and (3-5), it is concluded that assuming ω is real and considering the wave equation which includes damping is equivalent to assuming that ω is complex and considering the wave equation without damping, if $Im\omega > 0$. Therefore we should assume $Im\omega > 0$.

The sign of $Im\omega$ can also be determined through the causality condition which requires that no disturbance should be present before time $t = 0$. In order to satisfy this, the contour of inverse transform has to lie in the upper-half domain of the ω-plane, which indicates that $Im\omega > 0$. The causality condition will be discussed in Chapter 4.

Consideration of the radiation condition gives another way to determine the sign of $Im\omega$. Consider the branch cuts of γ_1 in the k-plane. For simplicity, assume $Re\omega > 0$. $Im\gamma_1$ must be positive according to the commitment made in Chapter 2. Two kinds of branch cuts are possible as shown in Figure 3-1. For the case $Im\omega > 0$, $Re\gamma_1$ is positive on the real axis and considering the form of the inverse transform:

$$\phi = \iint A(k,\omega) e^{i\gamma_1 y + ikx - i\omega t} \, d\omega dk \ , \tag{3-6}$$

this indicates the outgoing wave in y-direction. On the other hand, for the case $Im\omega < 0$, $Re\gamma_1$ is negative on the real axis, which indicates the incoming wave in y-direction. Therefore $Im\omega$ should be positive.

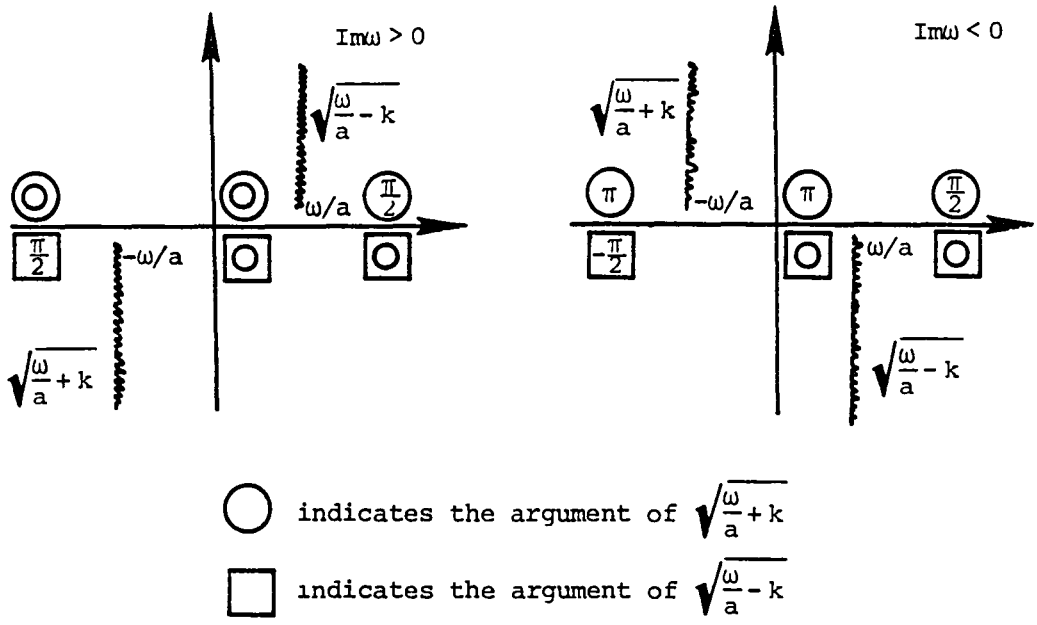

Figure 3-1 Branch Cuts of γ_1 in k-Plane

In all these methods, the common idea is to set a direction in time space, from the past to the future.

The poles of K are discussed in detail in Appendix A. The results are as follows: When $2 > M$, there are two complex poles at:

$$k = u(M)k_o \tag{3-7}$$

and

$$k = \overline{u(M)}k_o = u^*(M)k_o \tag{3-8}$$

where $\overline{u(M)}$ indicates the complex conjugate of u(M) and

$$u(M) = \frac{M + \sqrt{M^2+4-4\sqrt{M^2+1}}}{2\sqrt{M^2+1} - 2}, \tag{3-9}$$

$$k_o = \omega/a .$$

The poles $k = u(M)k_o$, $k = u^*(M)k_o$ are associated with instability of the vortex sheet when $M < 2\sqrt{2}$ and play a prominent role in the solution of the problem. They are therefore displayed explicitly by defining $\mu(k)$ by

$$K(k) = \frac{\gamma_1(k)\gamma_2(k)}{\mu(k)\ (k-u(M)k_o)\ (k-u^*(M)k_o)} . \tag{3-10}$$

We seek the radiating acoustic solutions that decay like

$$e^{-Imk_o|x|}$$

or

$$e^{-Imk_o|x|/(1\pm M)}$$

as $x \to \pm\infty$. Thus, all plus functions, denoted by a subscript +, will be analytic in the region

$$Imk < \frac{Imk_o}{1+M} , \tag{3-11}$$

while all minus functions, denoted by a subscript -, are analytic for k in the region

$$Imk > - Imk_o . \tag{3-12}$$

There is evidently a strip

$$\frac{Imk_o}{1+M} > Imk > - Imk_o \qquad : \text{ Region A} \tag{3-13}$$

in which full-range transforms of ϕ_1, ϕ_2, and h are analytic functions of k.

We consider the case $M < 1$. In this problem the branch cuts of γ_1 and γ_2 should take the form as shown in Figure 3-2 to satisfy the commitment that $Im\gamma_1$ and $Im\gamma_2$ must be positive on the real axis. The branch cuts of $\sqrt{k_o - Mk + k}$ and $\sqrt{k_o + k}$ lie in Region B and the branch cuts of $\sqrt{k_o - Mk - k}$ and $\sqrt{k_o - k}$ lie in Region C even though ω changes it value as long as $Im\omega > 0$, where Region B and Region C are defined as:

Region B: $\quad Imk < - Imk_o$

Region C: $\quad Imk > \dfrac{Imk_o}{1+M}$

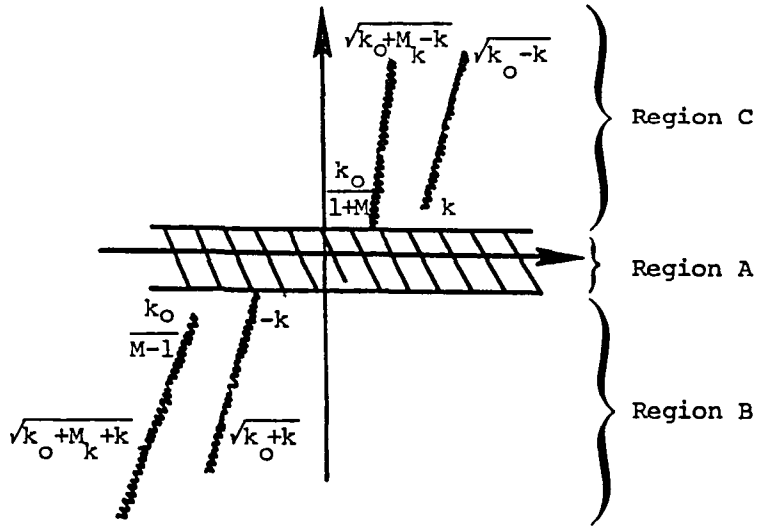

Figure 3-2 Branch Cuts and the Common Region of Analyticity

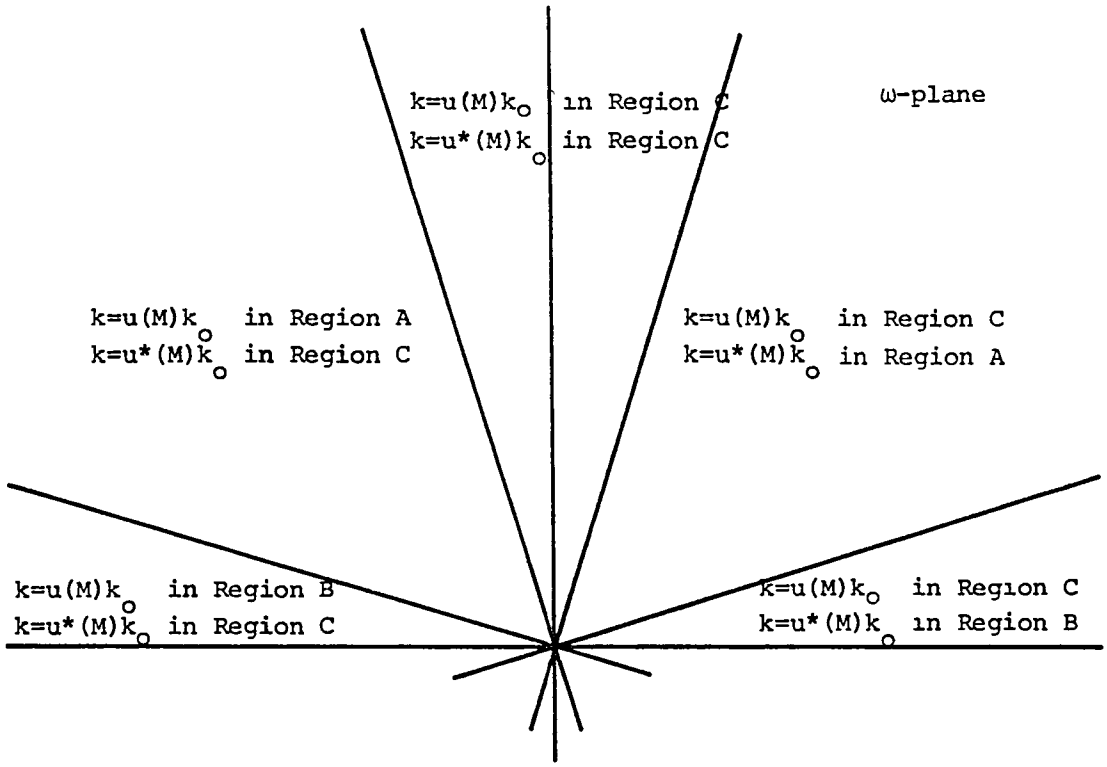

Figure 3-3 The Position of the Poles in the k-Plane According to the Value in the ω-Plane

The functions $\mu(k)$, γ_1, γ_2 are split into two parts such that:

$$\mu(k) = \mu_+(k)/\mu_-(k) \ , \qquad \gamma_1 = \gamma_{1-}/\gamma_{1+}, \quad \gamma_2 = \gamma_{2-}/\gamma_{2+} \ .$$

From the branch cuts we made previously it is apparent that

$$\left.\begin{aligned} \gamma_{1+}(k) &= (k_o - k)^{-1/2} \\ \gamma_{1-}(k) &= (k_o + k)^{1/2} \\ \gamma_{2+}(k) &= (k_o - Mk - k)^{-1/2} \\ \gamma_{2-}(k) &= (k_o - Mk + k)^{1/2} \ . \end{aligned}\right\} \qquad (3\text{-}14)$$

The calculation of $\mu_+(k)$ and $\mu_-(k)$ is presented in Appendix B. The difficulty arises from the poles $k = u(M)k_o$ and $k = u^*(M)k_o$. As can be seen in Figure 3-3, the position of the poles in the k-plane changes according to the value of ω. As a result, we cannot determine whether the terms $\left[k - u(M)k_o\right]$, $\left[k - u^*(M)k_o\right]$ work as a plus function or a minus function.

CHAPTER 4

CAUSALITY AND RADIATION CONDITION

The causality condition requires that no disturbance be present before time $t = 0$. Let the transformed solution have two poles at $k = u(M)k_o$ and $k = u^*(M)k_o$, which is the case in our problem. First, consider the inverse transform with respect to ω, assuming that k is real. It is apparent that to satisfy causality, the contour must lie above all the singularities in the ω-plane. In other words, the contour is deformed so that it always includes poles as shown in Figure 4-1. Then the branch cuts are constructed so that the radiation condition is satisifed along its contour; namely,

$\mathrm{Im}\gamma_1 > 0$ along the real axis and the position of the pole enclosed by the deformed contour, (4-1a)

$\mathrm{Re}\omega \cdot \mathrm{Re}\gamma_1 > 0$ along the real axis and the position of the pole enclosed by the deformed contour. (4-1b)

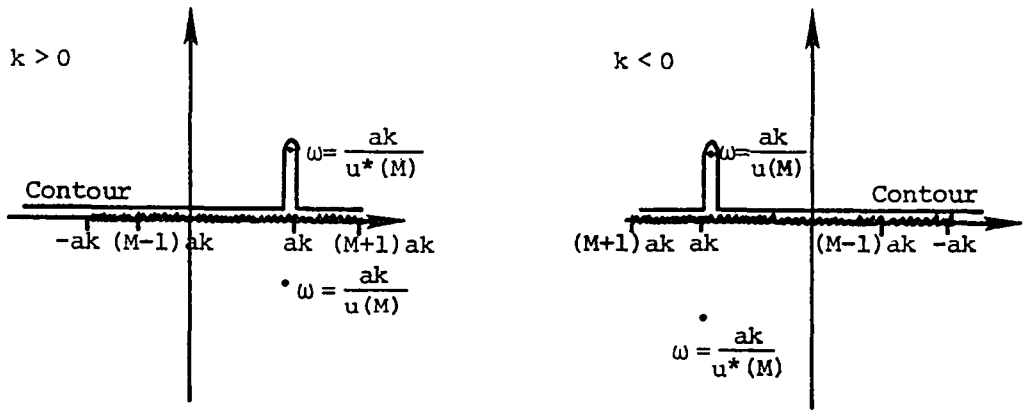

Figure 4-1 Contour of Integration and Branch Cuts in ω-Plane

The condition (4-1b) indicates that the solution leads to outgoing waves in $y > 0$. It is not easy to express the radiation condition for $y < 0$ because of the moving fluid. However, one can determine the branch cuts of γ_2 in such a way that when $M \to 0$ they coincide with those of γ_1. These branch cuts are also shown in Figure 4-1. To obtain the final result, integration is carried out with respect to k along the real axis.

Next, consider the inverse transform with respect to k, first assuming that ω is real or has a very small positive imaginary part.

$$\bar{f}(x,\omega) = \int_{C_k} \bar{\bar{f}}(k,\omega) e^{ikx} dk \ . \tag{4-2}$$

If we integrate it along the real axis, $\bar{f}(x,\omega)$ has singularities in the ω-plane when the poles $k = u(M)k_o$, $k = u^*(M)k_o$ hit the contour as ω changes its value as can be seen in Figure 4-2.

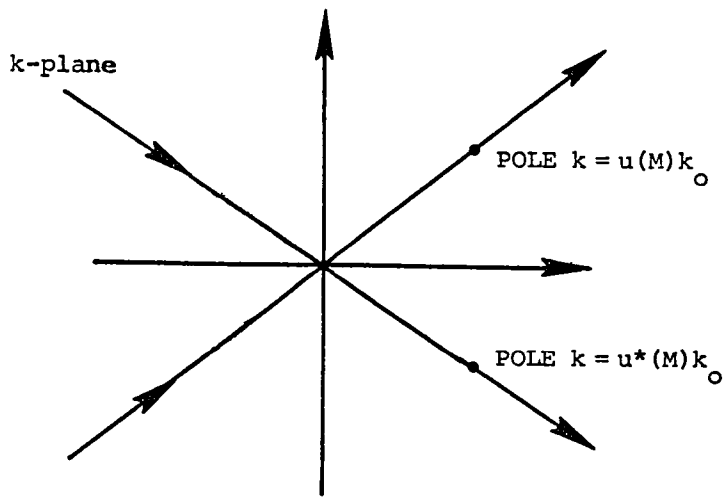

Figure 4-2 Movement of the Poles as ω Changes from $-\infty$ to ∞

There is no proper contour in the ω-plane which satisfies causality because of these singularities. To overcome this, the contour C_k is deformed in such a way that after the pole hits the real axis in the k-plane, the contour always includes this pole as shown in Figure 4-3 and as a result the singularities disappear. The branch cuts in the k-plane have already been made in Chapter 3 and along the real axis the conditions (4-1) are satisifed. We have no choice in making the branch cuts to satisfy conditions (4-1) at the position of the pole enclosed by the deformed contour except for the geometrical relation between the branch cuts and the poles. However, we have a choice in the deformation of the contour. The contour may be deformed to include the pole in the upper-half plane as shown in Figure 4-3(a), or the contour may be deformed to include the pole in the lower-half plane as shown in Figure 4-3(b).

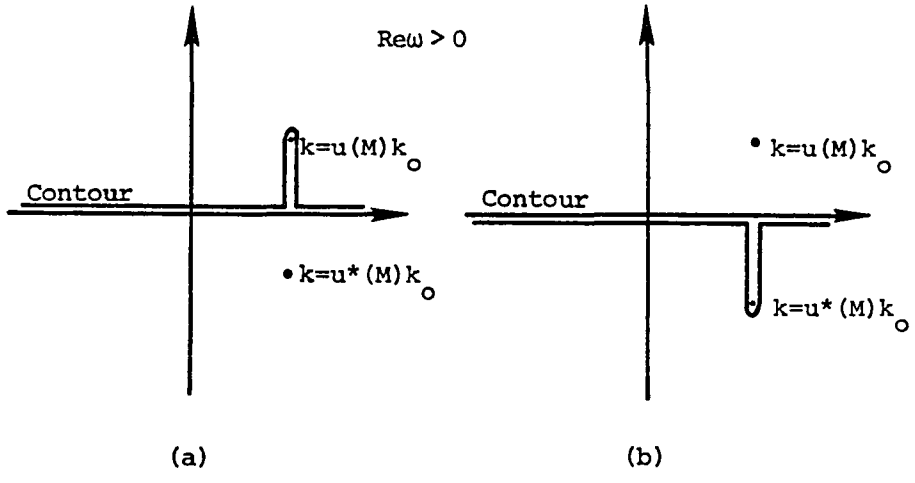

Figure 4-3 Contour of Integration in k-Plane when Reω > 0

Consider the case $\mathrm{Re}\omega > 0$. The relation between the two branch cuts of γ_1 and two poles is as Case I or Case II shown in Figure 4-4(a). According to the branch cuts defined in Chapter 3 at the pole $k = u(M)k_o$ we have:

Case I

$$\arg(k_o - k)^{1/2} = \frac{\pi}{2} + \frac{\theta_a}{2} \qquad \text{with} \quad \frac{\pi}{2} > \theta_a > 0 \tag{4-3a}$$

$$\arg(k_o + k)^{1/2} = \frac{\theta_b}{2} \qquad \text{with} \quad \frac{\pi}{2} > \theta_b > 0 \tag{4-3b}$$

and

$$\arg \gamma_1 = \frac{\pi + \theta_a + \theta_b}{2} \tag{4-3c}$$

$$\pi > \arg \gamma_1 > \frac{\pi}{2}\,, \tag{4-3d}$$

Case II

$$\arg(k_o - k)^{1/2} = -\frac{\pi}{2} + \frac{\theta_a}{2} \tag{4-4a}$$

$$\arg(k_o + k)^{1/2} = \frac{\theta_b}{2} \tag{4-4b}$$

and

$$\arg \gamma_1 = \frac{-\pi + \theta_a + \theta_b}{2} \tag{4-4c}$$

$$0 > \arg \gamma_1 > -\frac{\pi}{2}\,. \tag{4-4d}$$

Therefore at the pole $k = u(M)k_o$, condition (4-1a) is satisifed but (4-1b) is not satisfied in Case I, and condition (4-1b) is satisifed but (4-1a) is not satisfied in Case II.

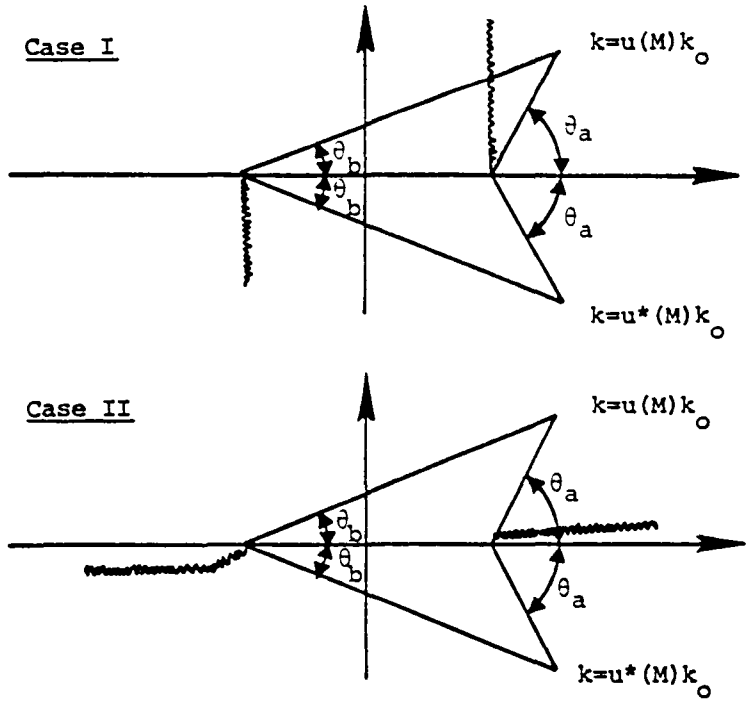

(a) Reω > 0

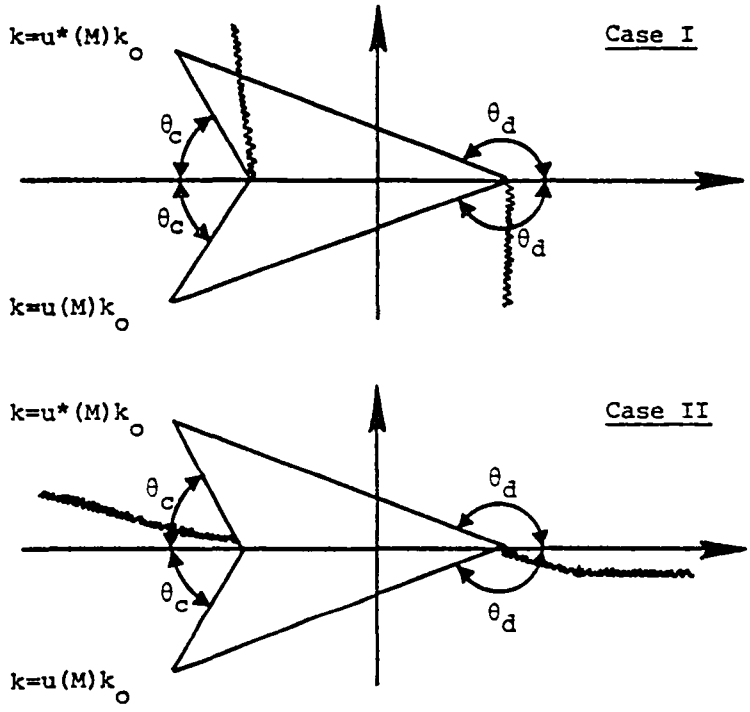

(b) Reω < 0

Figure 4-4 Relation Between Branch Cuts and Poles

At the pole $k = u(M)*k_o$, both Case I and Case II give:

$$\arg(k_o - k)^{1/2} = \frac{\pi}{2} - \frac{\theta_a}{2} \tag{4-5a}$$

$$\arg(k_o + k)^{1/2} = -\frac{\theta_b}{2} , \tag{4-5b}$$

and

$$\arg \gamma_1 = \frac{\pi - \theta_a - \theta_b}{2} \tag{4-5c}$$

$$\frac{\pi}{2} > \arg \gamma_1 > 0 . \tag{4-5d}$$

Therefore, at the pole $k = u^*(M)k_o$, γ_1 satisfies both conditions (4-1a) and (4-1b).

Next, consider the case $Re\omega < 0$. The relation between the branch cuts and two poles is as shown in Figure 4-4(b). Similarly, according to the branch cuts defined in Chapter 3 at the pole $k = u^*(M)k_o$ we have:

Case I

$$\arg(k_o - k)^{1/2} = \frac{-\theta_c}{2} \qquad \text{with} \quad \frac{\pi}{2} > \theta_c > 0 \tag{4-6a}$$

$$\arg(k_o + k)^{1/2} = \frac{\theta_d}{2} \qquad \text{with} \quad \pi > \theta_d > \frac{\pi}{2} \tag{4-6b}$$

and

$$\arg \gamma_1 = \frac{\theta_d - \theta_c}{2} \tag{4-6c}$$

$$\frac{\pi}{2} > \arg \gamma_1 > 0 , \tag{4-6d}$$

Case II

$$\arg(k_o - k)^{1/2} = \pi - \frac{\theta_c}{2} \tag{4-7a}$$

$$\arg(k_o + k)^{1/2} = \frac{\theta_d}{2} \tag{4-7b}$$

and

$$\arg \gamma_1 = \frac{2\pi - \theta_c + \theta_d}{2} \tag{4-7c}$$

$$\frac{3}{2}\pi > \arg \gamma_1 > \pi \ . \tag{4-7d}$$

At the pole $k = u^*(M)k_o$, condition (4-1a) is satisfied but (4-1b) is not satisfied in Case I, and condition (4-1b) is satisifed but (4-1a) is not satisifed in Case II.

At the pole $k = u(M)k_o$, both Case I and Case II give:

$$\arg(k_o - k)^{1/2} = \frac{\theta_c}{2} \tag{4-8a}$$

$$\arg(k_o + k)^{1/2} = \pi - \frac{\theta_d}{2} \tag{4-8b}$$

and

$$\arg \gamma_1 = \frac{2\pi + \theta_c - \theta_d}{2} \tag{4-8c}$$

$$\pi > \arg \gamma_1 > \frac{\pi}{2} \ . \tag{4-8d}$$

Therefore, at the pole $k = u(M)k_o$, γ_1 satisfies both conditions (4-1a) and (4-1b).

It is concluded that if we deform the contour so that all the poles are above the contour, radiation conditions (4-1) are satisfied at the position of the poles $k = u(M)k_o$, $k = u^*(M)k_o$, as well as along the real axis, whereas if we deform the contour so that all the poles are below the contour, radiation conditions are not satisfied. Therefore, the contour must be deformed to include all the poles above it.

It is obvious that the contour obtained here is also valid for the infinite vortex sheet problem and it is easily shown that the contribution from these poles coincides with the homogeneous solution obtained by Jones et al. [1-5].

The decomposition of the functions in the Wiener-Hopf technique is slightly changed. As the contour of inverse transform must lie in the common region of analyticity, the common region of analyticity has to be deformed in a similar way. Plus functions are defined as the functions which are analytic below the contour and minus functions are defined as the functions which are analytic above the contour. Then the decomposition of K(k) is determined uniquely as follows:

$$K_+ = \gamma_{1+}\,\gamma_{2+}\,\mu_+(k)\quad\left\{k-u(M)k_o\right\}\,\left\{k-u^*(M)k_o\right\} \tag{4-9a}$$

$$K_- = \gamma_{1-}\,\gamma_{2-}\,\mu_-(k)\ . \tag{4-9b}$$

CHAPTER 5

THE CONDITIONS AT THE PLATE EDGE AND THE VALUE OF THE ENTIRE FUNCTION

The Wiener-Hopf equation is given in Chapter 2 as:

$$\omega\overline{\overline{h}}_+K_+ + F_+ = K_-\left(\alpha\overline{\overline{\phi}}_{2-}\Big|_{y=0} - \overline{\overline{\phi}}_{1-}\Big|_{y=0} - L_1\right) - F_- = C(k) \tag{5-1}$$

where

$$\alpha = 1 - \frac{Vk}{\omega}$$

$$L_1 = -\frac{Vi}{2\pi\omega}\ \overline{\phi}_2(x,\omega)\Big|_{x=0,y=0} .$$

C(k) is the entire function of k and plus functions and minus functions are analytic below and above the contour determined in Chapter 4, respectively. Near the edge of the plate at the origin we assume:

$$\overline{\phi}_1(x,\omega) \to C_1(\omega) \qquad \text{as} \quad x \to -0 \quad \text{on} \quad y = +0 \tag{5-2a}$$

$$\overline{\phi}_2(x,\omega) \to C_2(\omega) \qquad \text{as} \quad x \to -0 \quad \text{on} \quad y = -0 \tag{5-2b}$$

$$\overline{\phi}_2(x,\omega) - \overline{\phi}_2(0,\omega) = 0(x^{\ell_1}) \qquad \text{as} \quad x \to +0 \quad \text{on} \quad y = -0 \tag{5-2c}$$

$$\overline{h}(x,\omega) = 0(x^{\ell_2}) \qquad \text{as} \quad x \to +0 \quad \text{on} \quad y = +0 \tag{5-2d}$$

where $\ell_1 \geq 1$, $\ell_2 > 0$. In these conditions, the expression $x \to -0$, $y = +0$, for example, means that x tends to zero through negative value of x on the upper side of the plate. The $C_i(\omega)$ are functions of ω and need not be known explicitly.

The third condition indicates that the x-component of the disturbed velocity is finite below the vortex sheet at the edge. The fourth condition is the requirement that the vortex sheet should attach to the edge of the plate.

Carrying out the half-range Fourier transform defined by Eq. (2-7), the asymptotic behavior of the above functions can be calculated with the aid of the Abelian theorem as:

$$\bar{\bar{\phi}}_{1-}(k,\omega) = 0\left(|k|^{-1}\right) \qquad \text{as } k\to\infty \text{ in } \mathrm{Im}k > -\mathrm{Im}k_o \qquad (5\text{-}3a)$$

$$\bar{\bar{\phi}}_{2-}(k,\omega) = 0\left(|k|^{-1}\right) \qquad \text{as } k\to\infty \text{ in } \mathrm{Im}k > -\mathrm{Im}k_o \qquad (5\text{-}3b)$$

$$\bar{\bar{\phi}}_{2-}(k,\omega) - \frac{i\bar{\phi}_2(0,\omega)}{2\pi k} = 0\left(|k|^{-1-\ell_1}\right) \qquad \text{as } k\to\infty \text{ in } \mathrm{Im}k > -\mathrm{Im}k_o \qquad (5\text{-}3c)$$

$$\bar{\bar{h}}_{+}(k,\omega) = 0\left(|k|^{-1-\ell_2}\right) \qquad \text{as } k\to\infty \text{ in } \mathrm{Im}k < \frac{\mathrm{Im}k_o}{1+M}\,. \qquad (5\text{-}3d)$$

$F_+(k)$, $F_-(k)$ are given as follows:

$$F_+(k) = \frac{-1}{2\pi i}\int_{C_+} \frac{F(\lambda)}{\lambda-k}\,d\lambda \qquad (5\text{-}4a)$$

$$F_-(k) = \frac{1}{2\pi i}\int_{C_-} \frac{F(\lambda)}{\lambda-k}\,d\lambda \qquad (5\text{-}4b)$$

where

$$F(\lambda) = \frac{i\gamma_1(\lambda)\alpha e^{-i\left(\lambda x_o+\gamma_2(\lambda)y_o\right)}K_+}{4\pi^2a^2\left(\gamma_2(\lambda)+\gamma_1(\lambda)\alpha^2\right)} = \frac{i\mu_-(\lambda)\gamma_{1-}^2(\lambda)\gamma_{2+}(\lambda)\alpha e^{-i\left(\lambda x_o+\gamma_2(\lambda)y_o\right)}}{4\pi^2a^2}\,. \qquad (5\text{-}4c)$$

Since $F(\lambda)$ does not have a pole at $\lambda = u(M)k_o$ nor $\lambda = u^*(M)k_o$, the contour C_+ and C_- need not be deformed and lie in Region A defined in Chapter 3. C_+ passes above $\lambda = k$ while C_- passes below $\lambda = k$. The exponential decay of $F(\lambda)$ on the contour, since $Im\gamma_2 > 0$, $y_o < 0$ ensures that these integrals exist and that $F_+(k) = 0\left(|k|^{-1}\right)$, $F_-(k) = 0\left(|k|^{-1}\right)$ as $k \to \infty$ in respective regions. The asymptotic behavior of $\mu_+(k)$, $\mu_-(k)$ is calculated in Appendix B as:

$$\mu_+(k) = 0\left(|k|^{1/2}\right) \qquad \text{as} \quad k \to \infty \quad \text{in} \quad Imk < \frac{Imk_o}{1+M} \tag{5-5a}$$

$$\mu_-(k) = 0\left(|k|^{-1/2}\right) \qquad \text{as} \quad k \to \infty \quad \text{in} \quad Imk > -Imk_o \,. \tag{5-5b}$$

Therefore, the asymptotic behavior of the known functions in the Wiener-Hopf equation can be estimated as follows:

$$K_+(k) = 0\left(|k|^{3/2}\right) \qquad \text{as } k \to \infty \quad \text{in} \quad Imk < \frac{Imk_o}{1+M} \tag{5-6a}$$

$$K_-(k) = 0\left(|k|^{1/2}\right) \qquad \text{as } k \to \infty \quad \text{in} \quad Imk > -Imk_o \tag{5-6b}$$

$$F_+(k) = 0\left(|k|^{-1}\right) \qquad \text{as } k \to \infty \quad \text{in} \quad Imk < \frac{Imk_o}{1+M} \tag{5-6c}$$

$$F_-(k) = 0\left(|k|^{-1}\right) \qquad \text{as } k \to \infty \quad \text{in} \quad Imk > -Imk_o \,. \tag{5-6d}$$

First we calculate the value of minus functions:

$$L_1 = -\frac{V_1}{2\pi\omega}\,\bar{\phi}_2(0,\omega)\Big|_{y=0}$$

$$= -\frac{Vk}{\omega}\,\bar{\bar{\phi}}_2(k,\omega)\Big|_{y=0} + 0\left(|k|^{-\ell_1}\right) \tag{5-7}$$

$$K_-\left(\alpha\bar{\bar{\phi}}_{2-}\Big|_{y=0} - \bar{\bar{\phi}}_{1-}\Big|_{y=0} - L_1\right) - F_- = K_-\left\{\bar{\bar{\phi}}_{2-}\Big|_{y=0} - \bar{\bar{\phi}}_{1-}\Big|_{y=0} + 0\left(|k|^{-\ell_1}\right)\right\} - F_-$$

$$= 0\left(|k|^{1/2-\ell_1}\right), \text{ as } k\to\infty \text{ in } \mathrm{Im}k > -\mathrm{Im}k_o\,. \tag{5-8}$$

As $\ell_1 \geq 1$, the value of the entire function $C(k)$ must be identically zero because of Liouville's theorem. Next, calculate plus functions

$$\omega\bar{\bar{h}}_+K_+ + F_+ = 0\left(|k|^{1/2-\ell_2}\right) \quad \text{as } k\to\infty \text{ in } \mathrm{Im}k < \frac{\mathrm{Im}k_o}{1+M}\,. \tag{5-9}$$

In order to make $C(k)$ equal zero, $\ell_2 > 1/2$. If we set $C(k) = 0$, then

$$\omega\bar{\bar{h}}_+ = \frac{-F_+}{K_+} = 0\left(|k|^{-5/2}\right) \quad \text{as } k\to\infty \text{ in } \mathrm{Im}k < \frac{\mathrm{Im}k_o}{1+M}\,, \tag{5-10}$$

which implies

$$\bar{h}(x,\omega) = 0\left(x^{3/2}\right)\,, \quad \text{as } x\to+0 \text{ on } y=0\,, \tag{5-11}$$

and as a result the slope of the vortex sheet becomes zero at the edge of the plate as well as the displacement of the vortex sheet (full Kutta condition).

CHAPTER 6

BEHAVIOR OF THE SOLUTION WHEN M TENDS TO ZERO

The behavior of the solution near the edge of the plate is different from that of the Sommerfeld half-plane diffraction problem (without the flow). Let us examine the y-component of the velocity on the vortex sheet near the edge of the plate.

$$K_+ = \gamma_{1+}\gamma_{2+}\mu_+(k)\left\{k - u(M)k_o\right\}\left\{k - u^*(M)k_o\right\}$$

$$= \gamma_{1+}\gamma_{2+}\left(\gamma_2+\gamma_1\alpha^2\right)\mu_-(k) \quad , \tag{6-1}$$

since

$$\mu_+(k) = \frac{\left(\gamma_2+\gamma_1\alpha^2\right)\mu_-(k)}{\left(k-u(M)k_o\right)\left(k-u^*(M)k_o\right)} . \tag{6-2}$$

The asymptotic behavior of $\mu_-(k)$ is given in Appendix B as:

$$\mu_-(k) = O\left(M^{-1}|k|^{-1/2}\right) ; \tag{6-3}$$

Hence

$$K_+(k) = O\left\{M^{-1}|k|^{-1/2}\left(1+M|k|+M^2|k|^2\right)\right\} . \tag{6-4}$$

The asymptotic behavior of $F_+(k)$ is given in Chapter 5 as:

$$F_+(k) = O\left(M^{-1}|k|^{-1}\right) . \tag{6-5}$$

Therefore in our problem

$$\frac{\partial \bar{\bar{\phi}}_{1+}}{\partial y} = 0\left\{|k|^{-1/2}\left(1+M|k|+M^2|k|^2\right)^{-1}\right\} \tag{6-6a}$$

$$\frac{\partial \bar{\bar{\phi}}_{2+}}{\partial y} = 0\left\{|k|^{-1/2}\left(1+M|k|\right)\left(1+M|k|+M^2|k|^2\right)^{-1}\right\} \tag{6-6b}$$

since

$$\frac{\partial \bar{\bar{\phi}}_{1+}}{\partial y} = -i\omega\bar{\bar{h}}_{+}$$

$$= \frac{iF_{+}}{K_{+}} \tag{6-7a}$$

and

$$\frac{\partial \bar{\bar{\phi}}_{2+}}{\partial y} = -i\omega\alpha\bar{\bar{h}}_{+}$$

$$= \frac{i\alpha F_{+}}{K_{+}} . \tag{6-7b}$$

Here the dependence of the asymptotic behavior on M is displayed explicitly. If M is finite

$$\frac{\partial \bar{\bar{\phi}}_{1+}}{\partial y} = 0\left(|k|^{-5/2}\right) \tag{6-8a}$$

$$\frac{\partial \bar{\bar{\phi}}_{2+}}{\partial y} = 0\left(|k|^{-3/2}\right) . \tag{6-8b}$$

Then the Abelian theorem implies

$$\frac{\partial\bar{\phi}_1}{\partial y} = O\left(x^{3/2}\right) \qquad \text{as} \quad x \to +0 \quad \text{on} \quad y = +0 \tag{6-9a}$$

$$\frac{\partial\bar{\phi}_2}{\partial y} = O\left(x^{1/2}\right) \qquad \text{as} \quad x \to +0 \quad \text{on} \quad y = -0 \ . \tag{6-9b}$$

In the Sommerfeld problem

$$\frac{\partial\bar{\bar{\phi}}_1}{\partial y} = \frac{\partial\bar{\bar{\phi}}_2}{\partial y} = O\left(|k|^{-1/2}\right) \tag{6-10}$$

and

$$\frac{\partial\bar{\phi}_1}{\partial y} = \frac{\partial\bar{\phi}_2}{\partial y} = O\left(x^{-1/2}\right) \qquad \text{as} \quad x \to +0 \quad \text{on} \quad y = 0 \ . \tag{6-11}$$

In these expressions the asymptotic behavior is calculated when $k \to \infty$ in the lower half-plane of the k-plane defined in each problem respectively. If $M \to 0$ and $Mk \to 0$, the asymptotic behavior of the two problems coincides. In other words, the existence of the flow smooths the edge behavior of the solution. In fact, for the small Mach number

$$u(M) \approx \frac{1+i}{M} \tag{6-12a}$$

$$u^*(M) \approx \frac{1-i}{M} \tag{6-12b}$$

and

$$\gamma_1^2(k) \approx \gamma_2^2(k) \approx k_o^2 - k^2 \tag{6-13a}$$

$$\gamma_{1+}(k) \approx \gamma_{2+}(k) \approx \left(k_o - k\right)^{-1/2} \tag{6-13b}$$

$$\gamma_{1-}(k) \approx \gamma_{2-}(k) \approx \left(k_o + k\right)^{1/2} \tag{6-13c}$$

$$\mu_-(k) \approx \frac{\left(k_o+k\right)^{-1/2}}{M} \tag{6-13d}$$

$$\mu_+(k) \approx \frac{\left(k_o-k\right)^{1/2}M}{k_o^2} . \tag{6-13e}$$

Hence

$$K_+(k) = \frac{M\left(k-u(M)k_o\right)\left(k-u^*(M)k_o\right)}{k_o^2\left(k_o-k\right)^{1/2}} \tag{6-14a}$$

$$F_+(k) = -\int_{C+} \frac{\alpha(\lambda)e^{-i\left(\lambda x_o+\gamma_2(\lambda)y_o\right)}d\lambda}{8\pi^3a^2\left(k_o-\lambda\right)^{1/2}(\lambda-k)M} \tag{6-14b}$$

$$\overline{\phi}_1(x,y,\omega) = -\int_{C_k}\int_{C_+} \frac{k_o^2\alpha(\lambda)e^{-i\left(\lambda x_o+\gamma_2(\lambda)y_o-kx-\gamma_1(k)y\right)}d\lambda dk}{8\pi^3a^2\left(k_o-\lambda\right)^{1/2}(\lambda-k)M^2\left(k-u(M)k_o\right)\left(k-u^*(M)k_o\right)\left(k_o+k\right)^{1/2}} . \tag{6-14c}$$

As $M \to 0$ and $Mk \to 0$,

$$\alpha \to 1 \tag{6-15a}$$

and

$$\frac{M^2(k-uk_o)(k-u^*k_o)}{k_o^2} = 1+\alpha^2 \to 2 . \tag{6-15b}$$

We have

$$\overline{\phi}_1(x,y,\omega) = -\int_{C_k}\int_{C_+} \frac{e^{-i\left(\lambda x_o+\gamma_1(\lambda)y_o-kx-\gamma_1(k)y\right)}}{16\pi^3 a^2\left(k_o-\lambda\right)^{1/2}\left(k_o+k\right)^{1/2}\left(\lambda-k\right)}\, d\lambda dk \ . \qquad (6\text{-}16)$$

The solution coincides with that of the Sommerfeld problem discussed in Appendix C.

CHAPTER 7

TRANSMITTED SOUND FIELD

The transmitted sound field is formally given by the equation

$$\phi_1 = \int_{C_\omega}\int_{C_k} \frac{F_+(k)}{\gamma_1 K_+} e^{ikx-i\omega t+i\gamma_1 y} dk d\omega \tag{7-1}$$

where C_k and C_ω are the contours discussed in Chapter 4 and

$$F_+(k) = \frac{-1}{2\pi i}\int_{C_+} \frac{F(\lambda)}{\lambda-k} d\lambda \tag{7-2a}$$

$$F(\lambda) = \frac{i\mu_-(\lambda)\gamma_{1-}(\lambda)\gamma_{2+}(\lambda)\alpha(\lambda)e^{-i\left(\lambda x_o+\gamma_2(\lambda)y_o\right)}}{4\pi^2 a^2} \tag{7-2b}$$

where C_+ passes above $\lambda = k$. If we change the contour of the integration so that C_+ passes below $\lambda = k$, the contribution from the pole $\lambda = k$ must be added to the integration, which gives

$$F_+(k) = F(k) - \frac{1}{2\pi i}\int_{C_+} \frac{F(\lambda)}{\lambda-k} d\lambda$$

$$= F(k) - F_-(k) \ . \tag{7-3}$$

The transmitted sound field ϕ_t due to F(k) is given as

$$\phi_t = \int_{C_\omega}\int_{C_k} \frac{i\gamma_1 - \gamma_{2+}\mu_-(k)\alpha e^{ikx-i\omega t+i\gamma_1 y-ikx_o-i\gamma_2 y_o}}{4\pi^2 a^2 \gamma_1 K_+} dkd\omega$$

$$= \int_{C_\omega}\int_{C_k} \frac{i\alpha e^{ikx-i\omega t+i\gamma_1 y-ikx_o-i\gamma_2 y_o}}{4\pi^2 a^2 (\gamma_2+\gamma_1\alpha^2)} dkd\omega \ , \qquad (7\text{-}4)$$

which is exactly the same as the solution for a doubly infinite vortex sheet problem without a rigid plate as can be shown in Appendix D. Therefore, $F_-(k)$ is considered to indicate the effect of a semi-infinite plate on the doubly infinite vortex sheet sound field.

In this chapter we carry out the integration (7-1) with respect to k. The integration with respect to ω is carried out in Chapter 9. The advantages of integrating with respect to k first are:

(i) After the integration with respect to k, the time harmonic solution is obtained. The time harmonic factor is assumed to be $e^{-i\omega t}$.

(ii) The geometrical relation between the source and the observer is more clearly investigated as will be shown later.

Introducing the new parameters

$$\zeta = k/k_o$$

$$\nu = \lambda/k_o \ , \qquad (7\text{-}5)$$

the time harmonic solution of the transmitted field can be written as:

$$\overline{\phi}_1(x,y,\omega) = -\iint_{C_\zeta}\int_{C_\nu} \frac{v_-(\nu)w_{1-}(\nu)w_{2+}(\nu)(1-M\nu)e^{-ik_o\left(\nu x_o+w_2(\nu)y_o-\zeta x-w_1(\zeta)y\right)}}{8\pi^3 a^2(\nu-\zeta)\left(\zeta-u(M)\right)\left(\zeta-u^*(M)\right)w_{1-}(\zeta)w_{2+}(\zeta)v_+(\zeta)}\,d\nu d\zeta \tag{7-6}$$

where $w_1(\zeta)$, $w_2(\zeta)$, $w_{1-}(\zeta)$, $w_{2+}(\zeta)$, $\nu_+(\zeta)$, and $\nu_-(\zeta)$ are the counterparts of $\gamma_1(k)$, $\gamma_2(k)$, $\gamma_{1-}(k)$, $\gamma_{2+}(k)$, $\mu_+(k)$, and $\mu_-(k)$, respectively, and are defined as:

$$w_1^2(\zeta) = 1-\zeta^2$$

$$w_2^2(\zeta) = (1-M\zeta)^2 - \zeta^2$$

$$w_{1-}(\zeta) = (1+\zeta)^{1/2}$$

$$w_{2+}(\zeta) = (1-M\zeta-\zeta)^{-1/2}$$

$$\ell n\nu_-(\zeta) = -\ell nM(1+\zeta)^{1/2} - \frac{1}{\pi}\int_{\frac{1}{M-1}}^{-1} \frac{\arctan\dfrac{\left(1-M^2\nu^2\right)|w_1(\nu)|}{|w_2(\nu)|} - \dfrac{\pi}{2}}{\nu-\zeta}\,d\nu$$

$$v_+(\zeta) = \frac{\left\{w_2(\zeta)+w_1(\zeta)(1-M\zeta)^2\right\}v_-(\zeta)}{\left(\zeta-u(M)\right)\left(\zeta-u^*(M)\right)}\,. \tag{7-7}$$

The branch cuts of $w_1(\zeta)$ lie from -1 to $-\infty$ and from 1 to ∞ and the branch cuts of $w_2(\zeta)$ lie from $\frac{1}{M-1}$ to $-\infty$ and from $\frac{1}{M+1}$ to ∞ in the ζ-plane, which correspond to the branch cuts of $\gamma_1(k)$ from $-k_o$ to $\infty e^{-i\beta}$ and from k_o to $\infty e^{i\beta}$, and the branch cuts of $\gamma_2(k)$ from $\frac{k_o}{M-1}$ to $\infty e^{-i\beta}$ and from $\frac{k_o}{1+M}$ to $\infty e^{i\beta}$ in the k-plane, where

$$\beta = \arg k_o\,. \tag{7-8}$$

Since this rotation of the branch cuts does not affect the radiation conditions as discussed in Chapter 4, this is permissible. The contours of the integration C_ν and C_ζ are shown in Figure 7-1. In the following figures we draw two contours on the same plane because after the integration with respect to ν, the pole $\nu = \zeta$ is the contour of the next integration and therefore their relation can be easily shown.

Let

$$x_o = -(1-M^2)\, r_o \cos\theta_o$$
$$y_o = -(1-M^2)^{1/2} r_o \sin\theta_o \ . \tag{7-9}$$

r_o and θ_o are given as:

$$r_o = \sqrt{\frac{x_o^2}{(1-M^2)^2} + \frac{y_o^2}{1-M^2}} \qquad r_o > 0$$
$$\theta_o = \arctan \frac{y_o \sqrt{1-M^2}}{x_o} \qquad \pi > \theta_o > 0 \ . \tag{7-10}$$

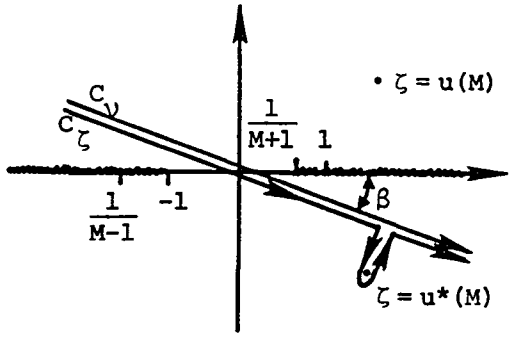

Figure 7-1 Branch Cuts and Integration Paths

Deform the contour C_ν into the curve $C\nu_1$ defined by

$$\nu = \frac{\cos(\theta_o + i\tau) - M}{1-M^2} \tag{7-11}$$

where τ is real and runs from $-\infty$ to ∞. This curve is a branch of a hyperbola with asymptotes $\nu = e^{\pm i\theta_o}$ and has a vertex at

$$\nu = \frac{\cos\theta_o - M}{1-M^2} . \tag{7-12}$$

This vertex lies between the branch point $\nu = -1$ and $\nu = \frac{1}{1+M}$ if

$$\cos\theta_o > M^2 + M - 1 . \tag{7-13}$$

Therefore, if Eq. (7-13) is satisifed, the contour can be deformed into the hyperbola without cutting the branch lines and we restrict the position of the line source in this region. The region expressed by Eq. (7-13) depends on the Mach number M, and as is shown in Figure 7-2, when M is small it covers almost all the moving flow and when M approaches 1 it is restricted to a small region.

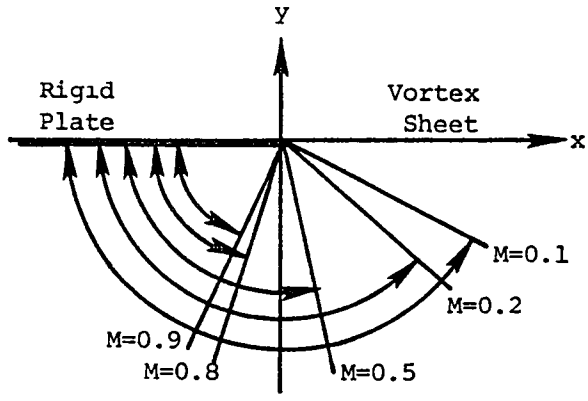

Figure 7-2 The Region Expressed by Eq. (7-13)

The contour of integration C_ζ is deformed in a similar way. Let

$$\left.\begin{aligned} x &= r\cos\theta \\ y &= r\sin\theta \end{aligned}\right\} \qquad (7\text{-}14)$$

with $r > 0$ and $\pi > \theta > 0$. Deform the contour C_ζ into the curve $C_{\zeta 1}$

$$\zeta = \cos(\theta + i\tau_1) \qquad (7\text{-}15)$$

where τ_1 is real and runs from $-\infty$ to ∞. This curve is a branch of a hyperbola with asymptotes $\zeta = e^{\pm i\theta}$ and has a vertex at

$$\zeta = \cos\theta \ . \qquad (7\text{-}16)$$

This vertex lies between the branch points $\zeta = -1$ and $\zeta = \frac{1}{1+M}$ if

$$\cos\theta < \frac{1}{1+M} \ . \qquad (7\text{-}17a)$$

If

$$\cos\theta < \frac{1}{1+M} \qquad (7\text{-}17b)$$

the contribution from the branch cut must be added. In both deformations, no contribution occurs from the linking arcs at infinity. Then on the contours the exponential part of the integration (7-6) becomes

$$-ik_o\left(\nu x_o + w_2(\nu) y_o - \zeta x - w_1(\zeta) y\right) = -ik_o\left(-r_o \cosh\tau + r_o M\cos\theta_o - r\cosh\tau_1\right) \ . \qquad (7\text{-}18)$$

The integration takes a different form according to the geometrical relation between the position of the line source and the observer as follows.

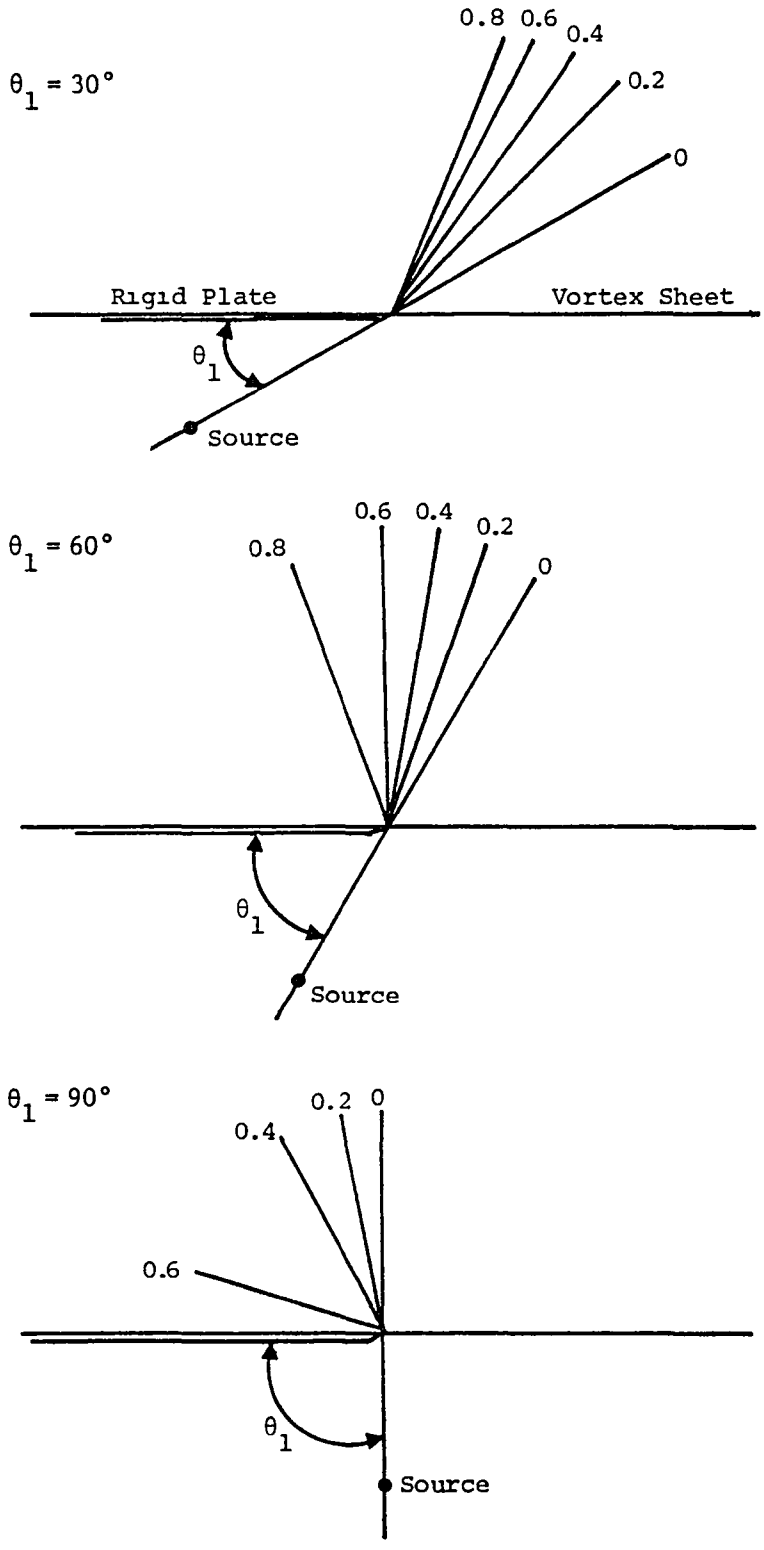

Figure 7-3 Region Expressed by Equation (7-21)

Region 1

When

$$\cos\theta < \frac{\cos\theta_o - M}{1-M^2} . \tag{7-19}$$

Introducing the real geometric angle and length defined by:

$$\left.\begin{aligned} x_o &= -r_1\cos\theta_1 \\ y_o &= -r_1\sin\theta_1 \end{aligned}\right\} \tag{7-20}$$

Eq. (7-19) can be written as:

$$\theta > \theta_2 \tag{7-21}$$

where

$$\cos\theta_2 = \frac{\cos\theta_1}{\sqrt{1-M^2\sin^2\theta_1}\,(1-M^2)} - \frac{M}{1-M^2} . \tag{7-21a}$$

The restriction of the angle (7-13) ensures that Eq. (7-21a) always has the root. The region expressed by Eq. (7-21) is shown in Figure 7-3.

If Eq. (7-19) is satisifed

$$\cos\theta_o > \cos\theta \tag{7-22}$$

since

$$\cos\theta_o > \frac{\cos\theta_o - M}{1-M^2} \tag{7-23}$$

is satisfied identically and hence

$$\theta_o < \theta . \tag{7-24}$$

As

$$\frac{\cos\theta_o - M}{1-M^2} < \frac{1}{1+M} \tag{7-25}$$

is also satisfied identically

$$\cos\theta < \frac{1}{1+M} \tag{7-26}$$

and hence no contribution occurs from the branch cut. The relation of the two contours is as shown in Figure 7-4.

The transmitted sound field $\overline{\phi}_1$ is given as:

$$\overline{\phi}_1(x,y,\omega) = \overline{\phi}_d(x,y,\omega) \tag{7-27}$$

where

$$\overline{\phi}_d = \int_{-\infty}^{\infty} \frac{F_o(\zeta) e^{ik_o r \cosh\tau_1}}{4\pi^2 a^2 (\zeta-u)(\zeta-u^*) w_{1+}(\zeta) w_{2+}(\zeta) v_+(\zeta)} d\tau_1 \tag{7-28}$$

and

$$F_o(\zeta) = \int_{-\infty}^{\infty} \frac{v_-(\nu) w_{1-}(\nu) w_{2-}(\nu)(1-M\nu) e^{ik_o r_o(\cosh\tau - M\cos\theta_o)}}{2\pi(\nu-\zeta)\sqrt{1-M^2}} d\tau . \tag{7-29}$$

If $C_{\nu 1}$ and $C_{\zeta 1}$ intersect as shown in Figure 7-4(b), which may occur when $\theta \approx \theta_2$, the contribution from the pole $\nu = \zeta$ must be added to give:

$$\overline{\phi}_1(x,y,\omega) = \overline{\phi}_d(x,y,\omega) + \overline{\phi}_s(x,y,\omega) \tag{7-30}$$

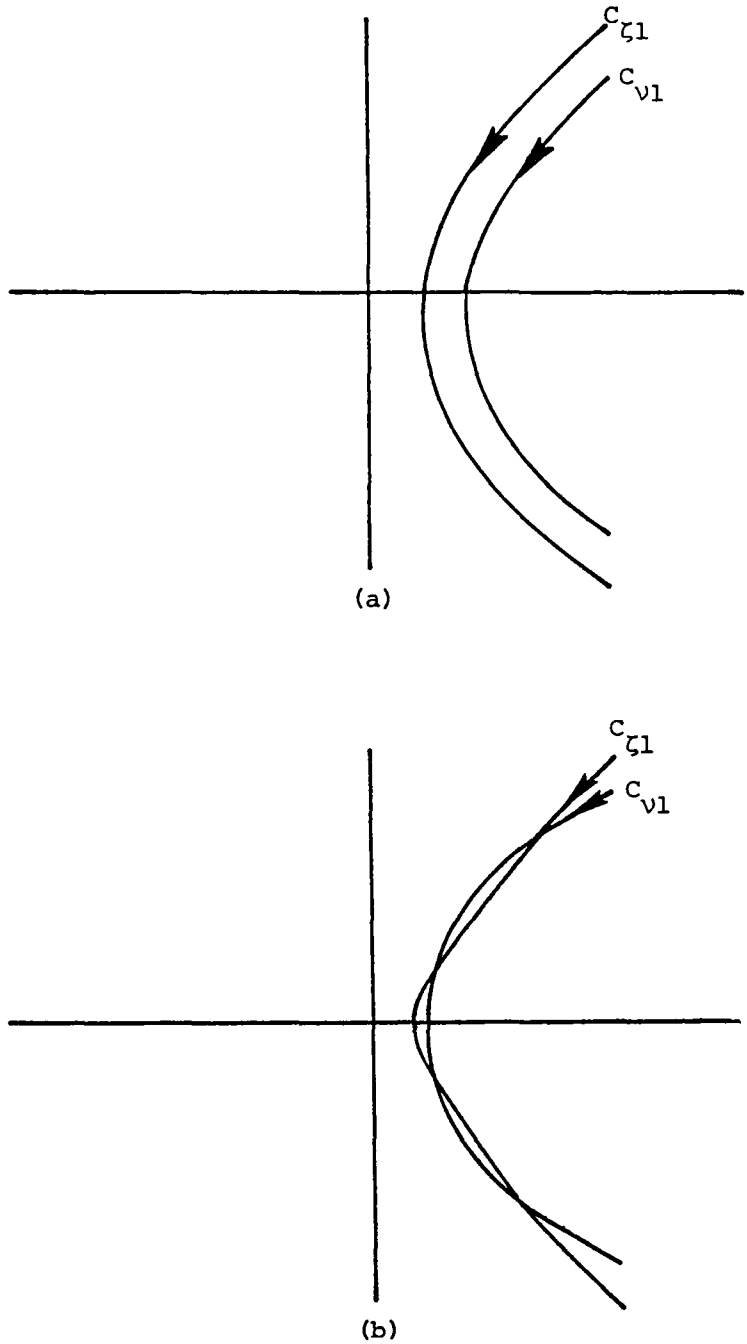

Figure 7-4 Relation Between $C_{\zeta 1}$ and $C_{\nu 1}$ $\theta > \theta_2$

where

$$\overline{\phi}_s = \int_{\lambda_2}^{\lambda_1} \frac{(1-M\zeta)w_1(\zeta)e^{ik_o\left(r\cosh\tau_1 - x_o - w_2(\zeta)y_o\right)}}{4\pi^2a^2\left\{w_2(\zeta)+w_1(\zeta)(1-M\zeta)^2\right\}} d\tau_1$$

$$+ \int_{\lambda_4}^{\lambda_3} \frac{(1-M\zeta)w_1(\zeta)e^{ik_o\left(r\cosh\tau_1 - \zeta x_o - w_2(\zeta)y_o\right)}}{4\pi^2a^2\left\{w_2(\zeta)+w_1(\zeta)(1-M\zeta)^2\right\}} d\tau_1 \quad . \tag{7-30a}$$

λ_1, λ_2, λ_3, and λ_4 are the roots of

$$\frac{\cos(\theta_o+i\tau)-M}{1-M^2} = \cos(\theta+i\tau_1) \tag{7-30b}$$

and

$$\lambda_1 > \lambda_2 > \lambda_3 > \lambda_4 \quad . \tag{7-30c}$$

Let

$$\cos(\theta_\zeta+i\tau_1) = u(M) \quad . \tag{7-31}$$

As shown in Appendix A, $\theta_3=\frac{\pi}{4}$. If $\theta < \theta_3$, the contribution from the poles $\zeta = u(M)$ and $\zeta = u^*(M)$ must be added to give

$$\overline{\phi}_1 = \overline{\phi}_d + H(\theta_\zeta-\theta)\overline{\phi}_{P1} \tag{7-32}$$

where

$$\overline{\phi}_{P1} = -\left.\frac{F_o(\zeta)e^{ik_o\left(\zeta x+w_1(\zeta)y\right)}}{2\pi a^2(\zeta-u^*)w_{1-}(\zeta)w_{2+}(\zeta)v_+(\zeta)}\right|_{\zeta=u}$$

$$-\left.\frac{F_o(\zeta)e^{ik_o\left(\zeta x+w_1(\zeta)y\right)}}{2\pi a^2(\zeta-u)w_{1-}(\zeta)w_{2+}(\zeta)v_+(\zeta)}\right|_{\zeta=u^*} . \tag{7-32a}$$

The relation between the poles and the contours is shown in Figure 7-5.

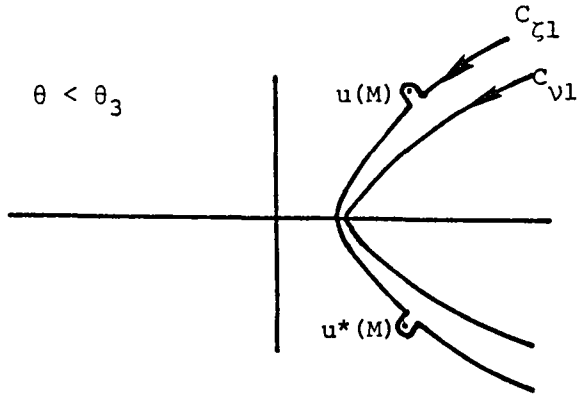

Figure 7-5 Relation Between the Poles and Contours

Region 2

When

$$\theta < \theta_o \ . \tag{7-33}$$

The region expressed by Eq. (7-33) is shown in Figure 7-6. If Eq. (7-33) is satisfied, then

$$\cos\theta > \frac{\cos\theta_o - M}{1-M^2} \ . \tag{7-34}$$

The relation between the two contours is as shown in Figure 7-7. When we deform the contour C_ζ to $C_{\zeta 1}$ the two contours intersect and the pole $\zeta = \nu$ brings another sound field $\overline{\phi}_t$ which is the same as the solution for the doubly infinite vortex sheet problem. In the calculation of $\overline{\phi}_t$ we are free to deform the contour if there is no contribution from the linking arcs at infinity as long as $C_{\nu 1}$ lies in the left of $C_{\zeta 1}$. We calculate $\overline{\phi}_t$ along the stationary path $\zeta(\sigma)$ which has its saddle point

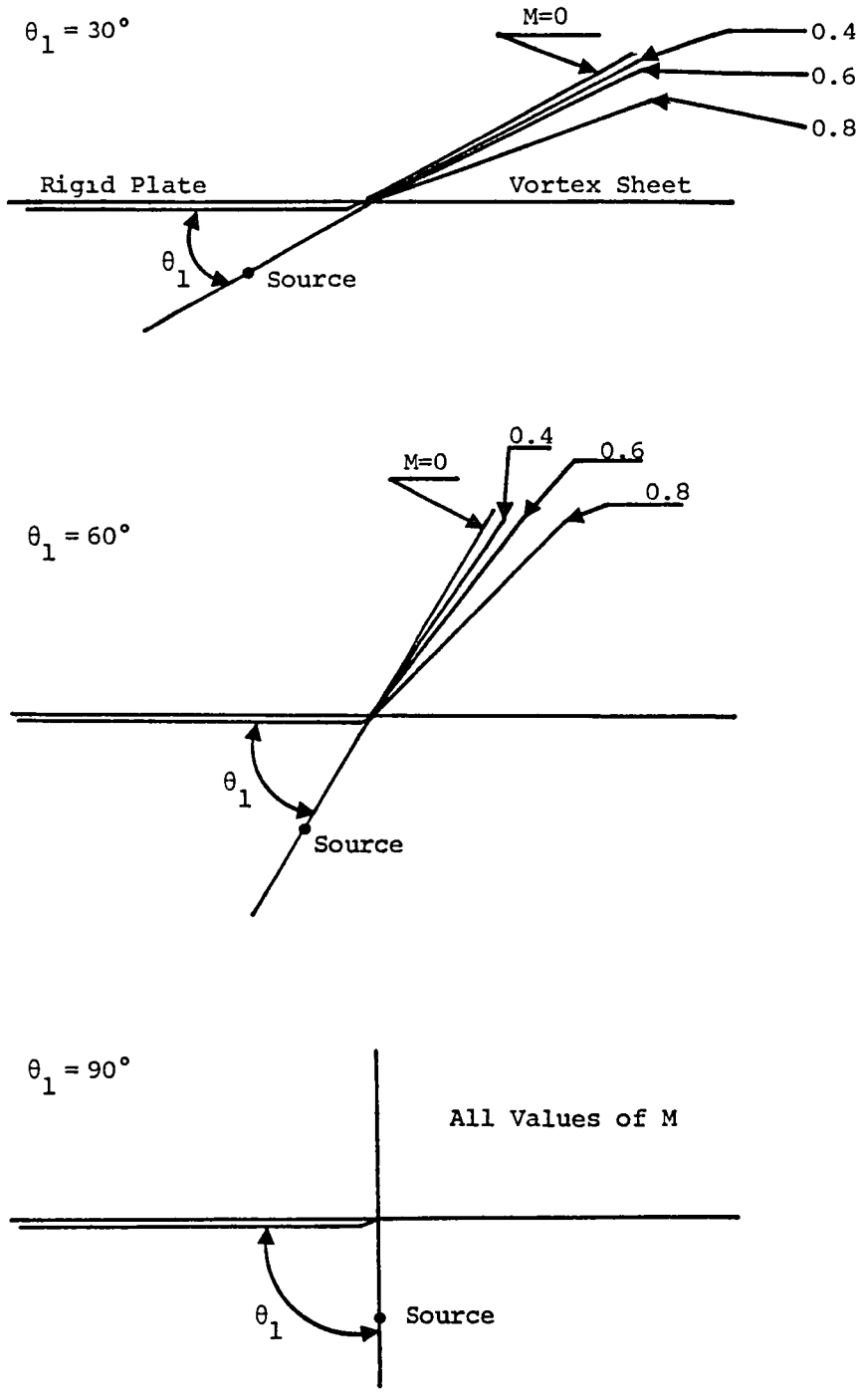

Figure 7-6 Region Expressed by Equation (7-33)

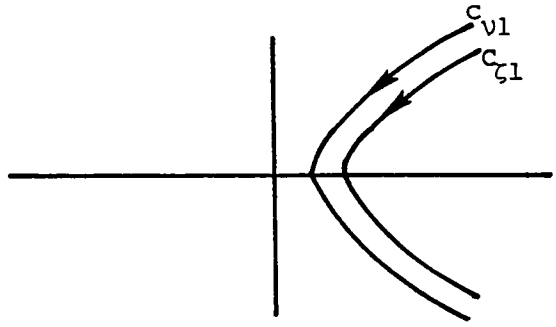

Figure 7-7 Relation Between $C_{\nu 1}$ and $C_{\zeta 1}$ $\theta < \theta_o$

between -1 and $\frac{1}{1+M}$ on the real axis and has its asymptotes $\zeta = e^{\pm\theta_4}$, where:

$$\theta_4 = \arctan \frac{-(1-M^2)^{1/2} y_o + y}{x - x_o} . \tag{7-35}$$

The character of $\zeta(\sigma)$ is discussed in detail in [1]. Then

$$\overline{\phi}_t = \int_{-\infty}^{\infty} \frac{i(1-M\zeta) e^{ik_o g(\sigma)}}{4\pi^2 a^2 \left\{ w_2(\zeta) + w_1(\zeta)(1-M\zeta)^2 \right\}} \frac{d\zeta}{d\sigma} \, d\sigma . \tag{7-36}$$

where

$$g(\sigma) = -\zeta x_o - w_2(\zeta) y_o + \zeta x + w_1(\zeta) y \qquad \mathrm{Im} g(0) = 0 . \tag{7-36a}$$

If $\zeta(\sigma)$ captures the poles u(M) and u*(M), another sound field $\overline{\phi}_{P2}$ must be added.

$$\overline{\phi}_{P2} = -\frac{(1-M\zeta)e^{ik_o\left(\zeta x+w_1(\zeta)y-\zeta x_o-w_2(\zeta)y_o\right)}}{2\pi a^2\frac{d}{d\zeta}\left\{w_2(\zeta)+w_1(\zeta)(1-M\zeta)^2\right\}}\Bigg|_{\zeta=u}$$

$$-\frac{(1-M\zeta)e^{ik_o\left(\zeta x+w_1(\zeta)y-\zeta x_o-w_2(\zeta)y_o\right)}}{2\pi a^2\frac{d}{d\zeta}\left\{w_2(\zeta)+w_1(\zeta)(1-M\zeta)^2\right\}}\Bigg|_{\zeta=u^*} . \qquad (7\text{-}37)$$

$\overline{\phi}_{P2}$ does not appear when $\theta_o < \theta_5$ where

$$\frac{\cos(\theta_5+i\tau_5)-M}{1-M^2} = u(M) . \qquad (7\text{-}38)$$

The relation between the contours and the poles is as shown in Figure 7-8. If $\theta < \theta_6$, where

$$\cos\theta_6 = (1+M)^{-1}, \qquad (7\text{-}39)$$

the contribution from the branch cut $\overline{\phi}_{b1}$ must be added.

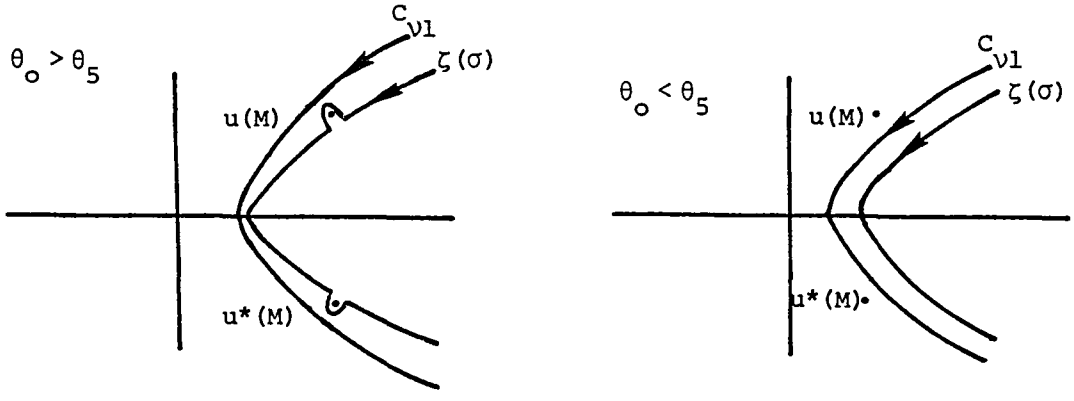

Figure 7-8 Relation Between the Poles and the Contours

$$\bar{\phi}_{b1} = \int_0^{i(\theta-\theta_6)} \left[\frac{F_o(\zeta) e^{ik_o r \cosh\tau_1}}{4\pi^2 a^2 (\zeta-u)(\zeta-u^*) w_{1+}(\zeta) w_{2+}(\zeta) v_+(\zeta)} \right]_- d\tau_1 . \qquad (7\text{-}40)$$

$[f(\zeta)]_- = f(\zeta+i\varepsilon) - f(\zeta - i\varepsilon)$ is the discontinuity of $f(\zeta)$ across the branch cut.

As a result, the transmitted sound field $\bar{\phi}_1$ in Region 2 is given as:

$$\bar{\phi}_1 = \bar{\phi}_d + H\left(\frac{\pi}{4} - \theta\right)\bar{\phi}_{P1} + H(\theta_6-\theta)\bar{\phi}_{b1} + \bar{\phi}_t + Q(M,x,y)H(\theta_o-\theta_5)\bar{\phi}_{P2} , \qquad (7\text{-}41)$$

where $Q(M,x,y)$ is 1 when $\zeta(\sigma)$ captures the poles and otherwise zero. $\bar{\phi}_t$, $\bar{\phi}_{P2}$ are the solutions for the doubly infinite vortex sheet problem (without rigid plate).

Region 3

When

$$\theta_2 > \theta > \theta_o . \qquad (7\text{-}42)$$

Region 3 is between Region 1 and 2, and is shown in Figure 7-9. The relation between the two contours is as shown in Figure 7-10. The contribution from the pole $\bar{\phi}_{t1}$ partially appears.

$$\bar{\phi}_{t1} = \int_{\lambda_5}^{\lambda_6} \frac{(1-M\zeta) w_1(\zeta) e^{ik_o\left(r\cosh\tau_1 - \zeta x_o - w_2(\zeta) y_o\right)}}{4\pi^2 a^2 \left\{ w_2(\zeta) + w_1(\zeta)(1-M\zeta)^2 \right\}} d\tau_1 . \qquad (7\text{-}43)$$

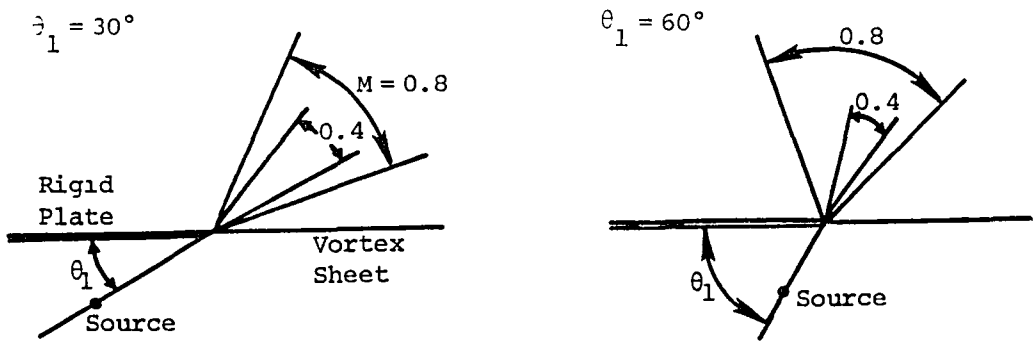

Figure 7-9 Region Expressed by Equation (7-42)

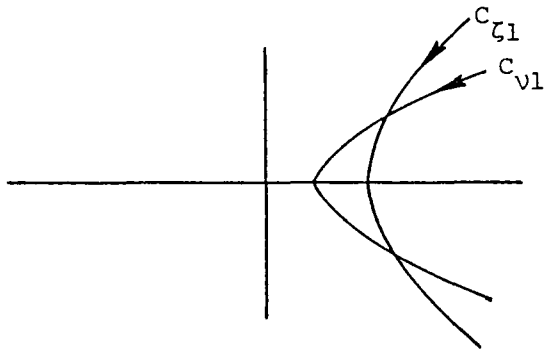

Figure 7-10 Relation Between $C_{\nu 1}$ and $C_{\zeta 1}$
$\theta_1 > \theta > \theta_o$

λ_5 and λ_6 are the roots of Eq. (7-30b), and

$$\lambda_6 > \lambda_5 \qquad \lambda_6 = -\lambda_5 \ . \tag{7-43a}$$

If $\theta < \theta_6$, the contribution from the branch cut $\overline{\phi}_{b2}$ must be added.

$$\overline{\phi}_{b2} = \int_0^{\imath(\theta-\theta_6)} \left[\frac{(1-M\zeta) w_1(\zeta) e^{\imath k_o \left(r\cosh\tau_1 - \zeta x_o - w_2(\zeta) y_o \right)}}{4\pi^2 a^2 \left\{ w_2(\zeta) + w_1(\zeta) (1-M\zeta)^2 \right\}} \right]_- d\tau_1 \ . \tag{7-44}$$

If $\theta < \frac{\pi}{4}$ and $\theta_o > \theta_5$, the contribution from the poles $\overline{\phi}_{P2}$ appears. As a result, the transmitted sound field $\overline{\phi}_1$ in Region 3 is given as:

$$\overline{\phi}_1 = \overline{\phi}_d + H\left(\frac{\pi}{4} - \theta\right) \overline{\phi}_{P1} + H(\theta_6 - \theta) \overline{\phi}_{b1} + \overline{\phi}_{t1} + H(\theta_6 - \theta) \overline{\phi}_{b2} + H\left(\frac{\pi}{4} - \theta\right) H(\theta_o - \theta_5) \overline{\phi}_{P2} \ . \tag{7-45}$$

CHAPTER 8

ASYMPTOTIC EVALUATION OF FAR FIELD

The fields $\bar{\phi}_d$, $\bar{\phi}_t$, $\bar{\phi}_{t1}$, $\bar{\phi}_{b1}$, and $\bar{\phi}_{b2}$ can be evaluated asymptotically under the assumption that $k_o r >> 1$ and $r >> r_o$. First consider the case when $\theta > \theta_6$. It is permissible to change the order of integration in integrating (7-28) and (7-29) because τ_1 and τ are real. Now assuming k_o is real and positive since $\tau_1 = 0$ is the saddle point, a standard stationary phase method is used to evaluate the integration to give:

$$\bar{\phi}_d = \left. \frac{F_o(\zeta) e^{ik_o r + \frac{\pi}{4} i}}{2\sqrt{2}\,\pi^{3/2} a^2 (\zeta - u)(\zeta - u^*) w_{1+}(\zeta) w_{2+}(\zeta) v_+(\zeta) \sqrt{k_o r}} \right|_{\zeta = \cos\theta} . \tag{8-1}$$

If $\theta < \theta_6$, $C_{\zeta 1}$ must be deformed to enclose the branch cut as shown in Figure 8-1, and special care must be taken since $w_{2+}(\zeta)$, $w_2(\zeta)$, $v_+(\zeta)$ take the different values depending on from which side ζ approaches to the branch cut.

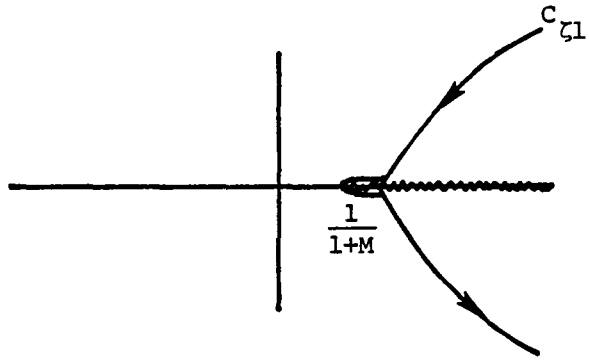

Figure 8-1 Deformation of $C_{\zeta 1}$ When $\theta < \theta_6$

$$\overline{\phi}_d + \overline{\phi}_{b1} = \int_{-\infty}^{\theta} \frac{F_o(\zeta) e^{ik_o r \cosh\tau_1}}{4\pi^2 a^2 (\zeta-u)(\zeta-u^*) w_{1+}(\zeta) w_{2+}(\zeta) v_+(\zeta)} d\tau_1$$

$$+ \int_0^{\infty} \frac{F_o(\zeta) e^{ik_o r \cosh\tau_1}}{4\pi^2 a^2 (\zeta-u)(\zeta-u^*) w_{1+}(\zeta) w_{2+}(\zeta) v_+(\zeta)} d\tau_1 + O\left(|k_o r|^{-3/2}\right)$$

$$= \frac{F_o(\zeta) e^{ik_o r + \frac{\pi}{4} i}}{4\sqrt{2}\, \pi^{3/2} a^2 (\zeta-u)(\zeta-u^*) w_{1+}(\zeta) \sqrt{k_o r}} \Bigg|_{\zeta=\cos\theta}$$

$$\left\{ \frac{1}{w_{2+}(\zeta) v_+(\zeta)} \Bigg|_{\zeta=-0+\cos\theta} + \frac{1}{w_2(\zeta) v_+(\zeta)} \Bigg|_{\zeta=+0+\cos\theta} \right\} + O\left(|k_o r|^{-3/2}\right), \tag{8-2}$$

where for example, $f(\zeta)\Big|_{\zeta=+0+a_o}$ means the value of $f(\zeta)$ when ζ approaches a_o through positive value on the upper side of the branch cut. As $\sigma = 0$ is the saddle point of integration (7-36), we have:

$$\overline{\phi}_t = \frac{i(1-M\zeta) e^{ik_o g(\sigma) + \operatorname{sgn} g''(\sigma) \frac{\pi}{4} i}}{2\sqrt{2}\, \pi^{3/2} a^2 \left\{ w_2(\zeta) + w_1(\zeta)(1-M\zeta)^2 \right\} \sqrt{k_o |g''(\sigma)|}} \frac{d\zeta}{d\sigma} \Bigg|_{\sigma=0}. \tag{8-3}$$

Since we assume $r >> r_o$, $\tau_1 = 0$ is the saddle point of integration (7-43) and the main contribution to the integration comes from this point. Therefore, asymptotically it is permissible to deform $C_{\zeta 1}$ to $\zeta(\sigma)$. We have

$$\overline{\phi}_t \approx \overline{\phi}_{t1} + \overline{\phi}_{b2} . \tag{8-4}$$

It is concluded that Region 2 and Region 3 asymptotically have the same character.

As we assume $r >> r_o$, both $C_{\zeta 1}$ and $\zeta(\sigma)$ have the same asymptotes and for small Mach number the poles are not included in the deformation from $C_{\zeta 1}$ to $\zeta(\sigma)$ if θ is not so close to $\frac{\pi}{4}$. Therefore, we have:

$$\overline{\phi}_t + Q(M,x,y)H(\theta_o-\theta_5)\overline{\phi}_{P2} = \overline{\phi}_t + H\left(\frac{\pi}{4}-\theta\right)H(\theta_o-\theta_5)\overline{\phi}_{P2}$$

$$= \overline{\phi}_{t1} + \overline{\phi}_{b2} + H\left(\frac{\pi}{4}-\theta\right)H(\theta_o-\theta_5)\overline{\phi}_{P2} . \quad (8-5)$$

CHAPTER 9

THE IMPULSIVE PROBLEM

In this chapter inverse transform with respect to ω is carried out to obtain the solution for the impulsive problem. $\phi_1(x,y,t)$ is formally given as:

$$\phi_1(x,y,t) = \int_{-\infty}^{\infty} \bar{\phi}_1(x,y,\omega) e^{-i\omega t} d\omega \tag{9-1}$$

where integration is carried out along the real axis in the ω-plane. In Region 1 we have

$$\phi_1 = \phi_d + H\left(\frac{\pi}{4} - \theta\right)\phi_{P1} \tag{9-2}$$

$$\phi_d = \int_{-\infty}^{\infty}\int_{-\infty}^{\infty} \frac{v_-(\nu) w_{1-}(\nu) w_{2-}(\nu) (1-M\nu) \delta\left\{t - \left(r_o \cosh\tau - r_o M \cos\theta_o + r\cosh\tau_1\right)/a\right\}}{4\pi^2 a^2 \sqrt{1-M^2}\ (\nu-\zeta)(\zeta-u)(\zeta-u^*) w_{1+}(\zeta) w_{2+}(\zeta) v_+(\zeta)} d\tau d\tau_1 \tag{9-3}$$

where the integration with respect to ω has been performed. This can be integrated with respect to either τ_1 or τ, but the remaining integration cannot be performed explicitly. It is however clear that ϕ_d vanishes for times $at < r_o - r_o M\cos\theta_o + r$. The arrival time of the wave front becomes earlier or later depending on the position of the line source due to the term $r_o M\cos\theta_o$ and hence the existence of the flow in the lower half-plane.

$$\phi_{Pl} = -\int_{-\infty}^{\infty}\int_{-\infty}^{\infty} \frac{v_-(\nu)w_{1-}(\nu)w_{2-}(\nu)(1-M\nu)e^{i\omega\left\{t-\left(r_o\cosh\tau - Mr_o\cos\theta_o + ux + w_1(u)y\right)/a\right\}}}{4\pi^2a^2(\nu-u)\sqrt{1-M^2}\,(u-u^*)w_{1-}(u)w_{2+}(u)v_+(u)}\,d\tau d\omega$$

$$-\int_{-\infty}^{\infty}\int_{-\infty}^{\infty} \frac{v_-(\nu)w_{1-}(\nu)w_{2-}(\nu)(1-M\nu)e^{i\omega\left\{t-\left(r_o\cosh\tau - Mr_o\cos\theta_o + u^*x + w_1(u^*)y\right)/a\right\}}}{4\pi^2a^2(\nu-u^*)\sqrt{1-M^2}\,(u^*-u)w_{1-}(u^*)w_{2+}(u^*)v_+(u^*)}\,d\tau d\omega\,. \tag{9-4}$$

It can be expressed in terms of the ultradistribution $\delta(z)$, where z is complex, as:

$$\phi_{Pl} = -\int_{-\infty}^{\infty} \frac{v_-(\nu)w_{1-}(\nu)w_{2-}(\nu)(1-M\nu)\delta\left\{t-\left(r_o\cosh\tau - Mr_o\cos\theta_o + ux + w_1(u)y\right)/a\right\}}{2\pi a^2(\nu-u)\sqrt{1-M^2}\,(u-u^*)w_{1-}(u)w_{2+}(u)v_+(u)}\,d\tau$$

$$-\int_{-\infty}^{\infty} \frac{v_-(\nu)w_{1-}(\nu)w_{2-}(\nu)(1-M\nu)\delta\left\{t-\left(r_o\cosh\tau - Mr_o\cos\theta_o + u^*x + w_1(u^*)y\right)/a\right\}}{2\pi a^2(\nu-u^*)\sqrt{1-M^2}\,(u^*-u)w_{1-}(u^*)w_{2+}(u^*)v_+(u^*)}\,d\tau\,. \tag{9-5}$$

The ultradistribution $\delta(z)$ has the property that

$$\delta(z) = \sum_{-\infty}^{\infty} (i\ \mathrm{Im}\ z)^n \delta^{(n)}(\mathrm{Re}z)/n! \tag{9-6}$$

and since generalized function $\delta^{(n)}(\mathrm{Re}z)$ vanishes for $\mathrm{Re}z \neq 0$, ϕ_{Pl} indicates the instability waves and vanishes for

$$\text{at} < r_o - Mr_o\cos\theta_o + \mathrm{Re}ux + \mathrm{Re}w_1(u)y\,. \tag{9-7}$$

It is easily checked that Reu, Reu*, $\mathrm{Rew}_1(u)$, and $\mathrm{Rew}_1(u^*)$ are all positive and these instability waves appear only in the downstream. Therefore ϕ_{P1} satisfies causality. On the other hand, if we deform the contour in the k-plane so that the two poles are always below the contour as discussed in Chapter 4, ϕ_{P1} appears in the upstream and for the certain value of negative x, ϕ_{P1} can be heard $t < 0$ and causality is violated.

In Region 2 we have

$$\phi_1 = \phi_d + H\left(\frac{\pi}{4} - \theta\right)\phi_{P1} + H(\theta_6-\theta)\phi_{b1} + \phi_t + Q(M,x,y)H(\theta_o-\theta_5)\phi_{P2} \tag{9-8}$$

$$\phi_{b1} = \int_{-\infty}^{\infty} \int_{0}^{1(\theta-\theta_6)} \left[\frac{v_-(\nu)w_{1-}(\nu)w_{2-}(\nu)(1-M\nu)\delta\left\{t-\left(r_o\cosh\tau - Mr_o\cos\theta_o + r\cosh\tau_1\right)/a\right\}}{4\pi^2a^2(\nu-\zeta)\sqrt{1-M^2}\,(\zeta-u)(\zeta-u^*)w_{1+}(\zeta)w_{2+}(\zeta)v_+(\zeta)} \right] d\tau_1 d\tau. \tag{9-9}$$

ϕ_{b1} can be integrated once only, but it is clear that it vanishes for times

$$at < r_o - Mr_o\cos\theta_o + r\cos(\theta_6-\theta) \ . \tag{9-10}$$

Since it is restricted to the region $\theta < \theta_6$, it is also causal. As indicated in Chapter 7, ϕ_t and ϕ_{P2} are the solution for the doubly infinite vortex sheet problem (without the rigid plate) which is calculated exactly and discussed in detail in [6]. The only difference is that the instability waves ϕ_{P2} are blocked and do not appear when $\theta_o < \theta_5$. In Region 3 the integration cannot be performed explicitly for ϕ_{t1} and ϕ_{b2}. However, as shown in Chapter 8, its nature is asymptotically the same as that of Region 2.

CHAPTER 10

CONCLUSIONS

The transmitted sound field ϕ_1 satisfies the full Kutta condition and causality condition.

The sound waves ϕ_d, ϕ_{Pl}, and ϕ_{bl} can be heard first at the edge of the plate at the time

$$t = (r_o - Mr_o\cos\theta_o)/a \tag{10-1}$$

which is the time that the emitted sound wave takes to travel from the source point to the plate edge in the moving fluid. This arrival time becomes earlier or later depending on whether the source is in the upstream $\left(\theta_o < \frac{\pi}{2}\right)$ or in the downstream of the plate edge $\left(\theta_o > \frac{\pi}{2}\right)$.

The field ϕ_d represents the field scattered from the edge of the plate and can be heard everywhere in $y > 0$. The wave front clearly occurs on the circle

$$r = at - r_o + Mr_o\cos\theta_o \tag{10-2}$$

and the time $t = (r + r_o - Mr_o\cos\theta_o)/a$ is the time for a signal to travel, via the edge, from the source to the observer.

ϕ_{bl} is the bow wave associated with ϕ_d and can be heard in the region $\theta < \theta_6$. Its wave front is expressed as:

$$at = r_o - r_o\cos\theta_o + r\cos(\theta_6 - \theta) \ . \tag{10-3}$$

This is the straight line from $x = (1+M)(at - r_o + Mr_o\cos\theta_o)$, $y = 0$, to the point of contact with the cylindrical diffracted wave front. ϕ_{P1} can be regarded as an instability wave triggered by the diffracted wave at the edge and is restricted to the region $\theta < \frac{\pi}{4}$. It exists in the triangular region bounded by the line $x = y$ and $Reux + Rew_1(u)y = at - r_o + Mr_o\cos\theta_o$.

The transmitted sound fields can be classified depending on how ϕ_t wave is transmitted. ϕ_t and ϕ_{P2} are the transmitted waves through the vortex sheet and are identical in the form to those found for the infinite vortex sheet.

In Region 1, ϕ_t is completely shaded by the rigid plate. In Region 2, ϕ_t is fully transmitted. Region 3 is the transition region between the two and ϕ_t is partially transmitted depending on its wave number.

If the observer is close to Region 1, ϕ_t is mostly shaded and if the observer is close to Region 2, ϕ_t is mostly transmitted. If the observer is far from the plate edge, the nature of the sound field is the same as that of Region 2.

ϕ_{P2} is another instability wave which occurs when $\zeta(\sigma)$ captures the poles. If the source is close to the rigid plate ($\theta_o < \theta_5$), this wave is blocked by the plate and does not appear.

If M tends to zero, the boundaries of Regions 1, 2, and 3 approach the diffracted angle of the Sommerfeld problem ($\theta_2 \to \theta_1$, $\theta_0 \to \theta_1$).

APPENDIX A

POLES OF K

The poles of K are given as the roots of the equation

$$\gamma_2(k) + \gamma_1(k)\alpha^2 = 0 \ . \tag{A-1}$$

Introducing the parameter

$$\zeta = ka/\zeta \ , \tag{A-2}$$

Eq. (A-1) reduces to the form:

$$\left\{w_1(\zeta) + w_2(\zeta)\right\} \left\{\zeta^2 + w_1(\zeta)w_2(\zeta)\right\} = 0 \tag{A-3}$$

where

$$\begin{aligned} w_1^2(\zeta) &= 1-\zeta^2 \\ w_2(\zeta) &= (1-M\zeta)^2 - \zeta^2 \end{aligned} \tag{A-4}$$

and to satisfy the sign convention of γ_1 and γ_2, the imaginary part of their counterparts w_1 and w_2 must have the same sign as k_o along the real axis. Accordingly, the branch cuts in the 3-plane are as shown in Figure A-1.

i) $$w_1(\zeta) + w_2(\zeta) = 0 \tag{A-5}$$

$$w_1^2(\zeta) = w_2^2(\zeta)$$

$$1 - \zeta^2 = (1-M\zeta)^2 - \zeta^2$$

$$(1 - 1 + M3)\ (1 + 1 - M3) = 0$$

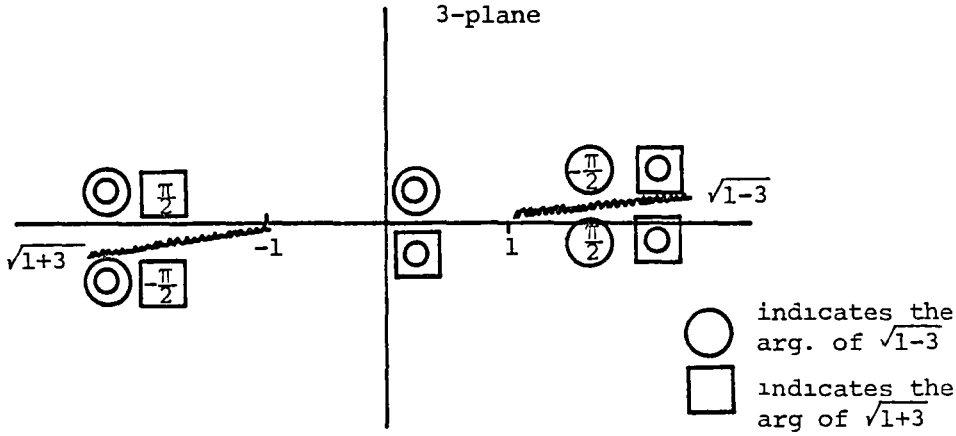

Figure A-1(a) Branch Cuts of $w_1(3)$

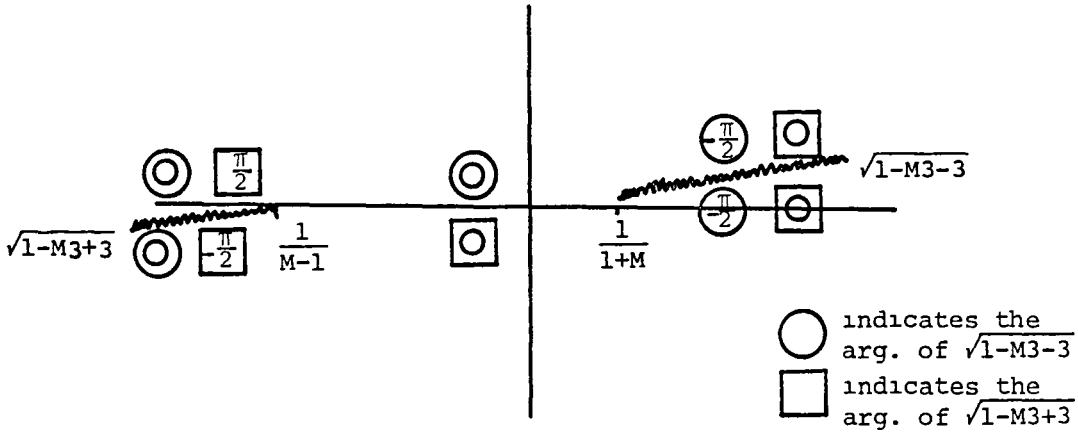

Figure A-1(b) Branch Cuts of $w_2(3)$

$$\zeta = 0$$

$$\zeta = \frac{2}{M} .$$

It is apparent that $\zeta = 0$ is not the solution of Eq. (A-5). If $M < 2$, $\zeta = \frac{2}{M}$ is situated on the right of $\zeta = 1$ and cannot be the solution of Eq. (A-5).

11) $\zeta^2 + w_1(\zeta)w_2(\zeta) = 0$ (A-6)

$$\zeta^4 = w_1^2(\zeta)w_2^2(\zeta)$$

$$1 - 2M\zeta + (M-2)\zeta^2 + 2M\zeta^3 - M^2\zeta^4 = 0$$

$$\left(\frac{1}{\zeta^2} - \frac{M}{\zeta} - 1\right)^2 - (M^2+1) = 0$$

$$\left(\frac{1}{\zeta^2} - \frac{M}{\zeta} - 1 - \sqrt{M^2+1}\right)\left(\frac{1}{\zeta^2} - \frac{M}{\zeta} - 1 + \sqrt{M^2+1}\right) = 0$$

$$\zeta = \frac{-M \pm \sqrt{M^2+4+4\sqrt{M^2+1}}}{2+2\sqrt{M^2+1}}$$

$$\zeta = \frac{M \pm \sqrt{M^2+4-4\sqrt{M^2+1}}}{2\sqrt{1+M^2} - 2}$$

$\zeta = \frac{-M+\sqrt{M^2+4+4\sqrt{1+M^2}}}{2+2\sqrt{M^2+1}}$ is between $\zeta = 0$ and $\zeta = \frac{1}{1+M}$. $\zeta = \frac{-M-\sqrt{M^2+4+4\sqrt{M^2+1}}}{2+2\sqrt{1+M^2}}$ is between $\zeta = 0$ and $\zeta = -1$. These two are not the solution of Eq. (A-6).

$\zeta = \frac{M\pm\sqrt{M^2+4-4\sqrt{M^2+1}}}{2\sqrt{1+M^2}-2}$ are the complex numbers which are situated above and below $\zeta = \frac{\sqrt{1+M^2}+1}{2M}$, respectively, when $M < 2\sqrt{2}$ and are the solution of Eq. (A-6).

These two solutions can be written as:

$$\zeta = \cos\left(\frac{1}{4}\pi \pm i\tau\right) \tag{A-7}$$

where τ is the positive root of the equation

$$\cosh\tau = \frac{1+\sqrt{1+M^2}}{\sqrt{2}\,M} . \tag{A-8}$$

APPENDIX B

CALCULATION OF $\mu_+(k)$ AND $\mu_-(k)$

As $\mu(k)$ does not have any zeros, $\mu_-(k)$ is defined by

$$\ell n\, \mu_-(k) = \frac{-1}{2\pi i} \int_{C_1} \frac{\ell n\, \mu(\lambda)}{\lambda - k}\, d\lambda \tag{B-1}$$

where C_1 passes below $\lambda = k$. Introducing the new parameters

$$\left.\begin{aligned} \zeta &= k/k_o \\ \nu &= \lambda/k_o \ , \end{aligned}\right\} \tag{B-2}$$

Eq. (B-1) can be written as

$$\ell n\, \mu_-(k) = \frac{-1}{2\pi i} \int_{C_2} \frac{\ell n\, \mu(\nu k_o)}{\nu - \zeta}\, d\nu \ . \tag{B-3}$$

The branch cuts of $w_1(\nu)$ lie from -1 to $-\infty$ and from 1 to ∞ and the branch cuts of $w_2(\nu)$ lie from $\frac{1}{M-1}$ to $-\infty$ and from $\frac{1}{M+1}$ to ∞ in the ν-plane as shown in Figure B-1 where $w_1(\nu)$ and $w_2(\nu)$ are the counterparts of $\gamma_1(k)$ and $\gamma_2(k)$ and are defined by:

$$\left.\begin{aligned} w_1^2(\nu) &= 1 - \nu^2 \\ w_2^2(\nu) &= (1 - M\nu)^2 - \nu^2 \ . \end{aligned}\right\} \tag{B-4}$$

The contour C_2 is distorted so that it is wrapped around the cut from -1 to $-\infty$. This process gives an additional contribution from the semicircle of radius R.

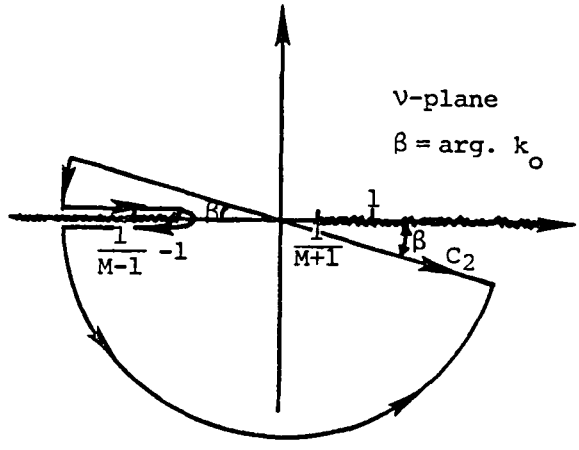

Figure B-1 Branch Cuts and Integration Paths

As $|\nu| \to \infty$ in the upper half-plane, $w_1 = -i\nu + 0(1)$, $w_2 = 0(|\nu|)$ and so

$$\mu(k) = \frac{-iM^2\nu}{k_o} + 0(1) \quad . \tag{B-5}$$

In the lower half-plane $w_1 = i\nu + 0(1)$, $w_2 = 0(|\nu|)$ and so

$$\mu(h) = \frac{iM^2\nu}{k_o} + 0(1) \quad . \tag{B-6}$$

It follows that the contribution from the semicircle is:

$$-\frac{1}{2\pi}\int_{\pi-\beta}^{\pi} \ell n\left(\frac{-iM^2Re^{i\theta}}{k_o}\right)\left(1+O(1/R)\right)d\theta - \frac{1}{2\pi}\int_{-\pi}^{-\beta} \ell n\left(\frac{iM^2Re^{i\theta}}{k_o}\right)\left(1+O(1/R)\right)d\theta$$

$$= -\frac{1}{2\pi}\left[\int_{\pi-\beta}^{\pi}\left\{\ell n\frac{M^2R}{k_o}+\frac{i}{k_o}\left(\theta-\frac{\pi}{2}\right)\right\}d\theta + \int_{-\pi}^{-\beta}\left\{\ell n\frac{M^2R}{k_o}+\frac{i}{k_o}\left(\theta+\frac{\pi}{2}\right)\right\} + O\left(\frac{\ell nR}{R}\right)\right.$$

$$= -\frac{1}{2}\ell n\frac{M^2R}{k_o} + O\left(\frac{\ell nR}{R}\right). \tag{B-7}$$

The discontinuity in $\ell n\mu(k)$ across the cut is:

$$\ell n\left\{\mu(k+i\varepsilon)/\mu(k-i\varepsilon)\right\} = \ell n\frac{w_2(\nu+i\varepsilon)+w_1(\nu+i\varepsilon)\alpha^2}{w_2(\nu-i\varepsilon)+w_1(\nu-i\varepsilon)\alpha^2}$$

$$= \begin{cases} \ell n(-1) = \pi i & \nu < \frac{1}{M-1} \\ \ell n\dfrac{\left(1-M^2\nu^2\right)|w_1|i+|w_2|}{-\left(1-M^2\nu^2\right)|w_1|i+|w_2|} = 2i\arctan\dfrac{\left(1-M^2\nu^2\right)}{|w_2|}|w_1| & \frac{1}{M-1} < \nu < -1. \end{cases} \tag{B-8}$$

$\ell n\mu_-(k)$ can be given as:

$$\ell n\mu_-(k) = -\frac{1}{2}\ell n\frac{M^2R}{k_o} - \frac{1}{2}\int_{-R}^{-1}\frac{d\nu}{\nu-\zeta} - \frac{1}{\pi}\int_{\frac{1}{M-1}}^{-1}\frac{\arctan\dfrac{\left(1-M^2\nu^2\right)|w_1|}{|w_2|}-\dfrac{\pi}{2}}{\nu-\zeta}d\nu$$

$$= -\frac{1}{2}\ell n\frac{M^2R}{k_o} - \frac{1}{2}\ell n(-1-\zeta) + \frac{1}{2}\ell n(-R) - \frac{1}{\pi}\int_{\frac{1}{M-1}}^{-1}\frac{\arctan\dfrac{\left(1-M^2\nu^2\right)|w_1|}{|w_2|}-\dfrac{\pi}{2}}{\nu-\zeta}d\nu$$

$$= -\ln \frac{M(1+\zeta)^{1/2}}{k_o^{1/2}} - \frac{1}{\pi} \int_{\frac{1}{M-1}}^{-1} \frac{\arctan \dfrac{\left(1-M^2\nu^2\right)|w_1|}{|w_2|} - \dfrac{\pi}{2}}{\nu-\zeta}\, d\nu \ . \qquad \text{(B-9)}$$

The asymptotic behavior of $\mu_-(k)$ as $|k| \to \infty$ is easily found as

$$\mu_-(k) = O\left(|k|^{-1/2}\right) \ . \qquad \text{(B-10)}$$

The identity $\mu_+(k) = \mu(k)\mu_-(k)$ can then be used to derive the corresponding results for $\mu_+(k)$ as follows:

$$\mu_+(k) = \frac{\left(\gamma_2 + \gamma_1\alpha^2\right)\mu_-(k)}{\left(k - u(M)k_o\right)\left(k - u^*(M)k_o\right)} \ . \qquad \text{(B-11)}$$

The asymptotic behavior of $\mu_+(k)$ is

$$\mu_+(k) = O\left(|k|^{1/2}\right) \ . \qquad \text{(B-12)}$$

APPENDIX C

SOLUTION FOR THE SOMMERFELD HALF-PLANE DIFFRACTION PROBLEM

Consider the case in which there is no flow in $y < 0$. The governing equations are:

$$\left.\begin{aligned} &\frac{\partial^2 \phi_2}{\partial t^2} - a^2 \nabla^2 \phi_2 = \delta(x - x_o)\, \delta(y - y_o)\, \delta(t) \qquad y < 0 \\ &\frac{\partial^2 \phi_1}{\partial t^2} - a^2 \nabla^2 \phi_1 = 0 \qquad\qquad\qquad\qquad\quad y > 0 \,. \end{aligned}\right\} \tag{C-1}$$

Carrying out the Fourier transform defined by Eq. (2-2), Eq. (C-1) reduces to the form:

$$\left.\begin{aligned} &\frac{\partial^2 \bar{\bar{\phi}}_2}{\partial y^2} + \gamma_1^2 \bar{\bar{\phi}}_2 = -\frac{\delta(y - y_o)}{4\pi^2 a^2}\, e^{-ikx_o} \\ &\frac{\partial^2 \bar{\bar{\phi}}_1}{\partial y^2} + \gamma_1^2 \bar{\bar{\phi}}_1 = 0 \end{aligned}\right\} \tag{C-2}$$

where

$$\gamma_1^2 = k_o^2 - k^2 \,, \qquad k_o = \omega / a \,.$$

Solutions to the set of ordinary differential Eq. (C-2) can be easily found as:

$$\left.\begin{aligned}
\bar{\bar{\phi}}_1 &= A_1(k,\omega)e^{i\gamma_1 y} + B_1(k,\omega)e^{-i\gamma_1 y} \\
\bar{\bar{\phi}}_2 &= A_2(k,\omega)e^{-i\gamma_1 y} + B_2(k,\omega)e^{-i\gamma_1 y} - \frac{e^{-ikx_o}}{4\pi^2 a^2 \gamma_1} \sin\left[\gamma_1(y-y_o)\right] H(y-y_o).
\end{aligned}\right\} \quad (C\text{-}3)$$

The sign convention of γ_1 is chosen such that the sign of its imaginary part is always positive and therefore B_1 and B_2 must be set to zero.

The boundary conditions at $y = 0$ are:

$$\frac{\partial \phi_1}{\partial t} = \frac{\partial \phi_2}{\partial t} \qquad x > 0 \quad \text{(continuity of pressure)} \qquad (C\text{-}4a)$$

$$\frac{\partial \phi_1}{\partial t} = \frac{\partial \phi_2}{\partial t} \qquad x > 0 \quad \text{(continuity of displacement)} \qquad (C\text{-}4b)$$

$$\frac{\partial \phi_1}{\partial y} \quad \frac{\partial \phi_2}{\partial y} = 0 \qquad x < 0 \quad \text{(rigid plate condition)} \; . \qquad (C\text{-}4c)$$

To express these conditions in the transformed region, carrying out the half-range Fourier transform defined by Eq. (2-7) we obtain:

$$\left.\begin{aligned}
\bar{\bar{\phi}}_{1+} &= \bar{\bar{\phi}}_{2+} \\
\frac{\partial \bar{\bar{\phi}}_{1+}}{\partial y} &= \frac{\partial \bar{\bar{\phi}}_{2+}}{\partial y} \\
\frac{\partial \bar{\bar{\phi}}_{1-}}{\partial y} &= \frac{\partial \bar{\bar{\phi}}_{2-}}{\partial y} = 0 \; .
\end{aligned}\right\} \quad (C\text{-}5)$$

Using the relation

$$\left.\begin{aligned} \frac{\partial \bar{\bar{\phi}}_1}{\partial y} &= \imath\gamma_1 \bar{\bar{\phi}}_1 \\ \frac{\partial \bar{\bar{\phi}}_2}{\partial y} &= -\imath\gamma_1 \bar{\bar{\phi}}_2 - \frac{e^{-\imath(kx_o+\gamma_1 y_o)}}{4\pi^2 a^2} , \end{aligned}\right\} \tag{C-6}$$

and eliminating all the unknown plus functions except for $\frac{\partial \bar{\bar{\phi}}_{1+}}{\partial y}$, we obtain:

$$2\,\frac{\partial \bar{\bar{\phi}}_{1+}}{\partial y} = \imath\gamma_1\left(\bar{\bar{\phi}}_{1-} - \bar{\bar{\phi}}_{2-}\right) - \frac{e^{-\imath(kx_o+\gamma_1 y)}}{4\pi^2 a^2} . \tag{C-7}$$

The branch cuts of γ_1 are the same as those defined in Chapter 3. The common region of analyticity is

$$\mathrm{Im}k_o > \mathrm{Im}k > -\mathrm{Im}k_o , \tag{C-8}$$

and $\mathrm{Im}\omega$ is kept to be positive. The function γ_1 is split into two parts such that $\gamma_1 = \gamma_{1-}/\gamma_{1+}$ where

$$\left.\begin{aligned} \gamma_{1+} &= \left(k_o - k\right)^{-1/2} \\ \gamma_{1-} &= \left(k_o + k\right)^{1/2} . \end{aligned}\right\} \tag{C-9}$$

Plus functions are analytic in the region $\mathrm{Im}k < \mathrm{Im}k_o$ and minus functions are analytic in the region $\mathrm{Im}k > -\mathrm{Im}k_o$. The Wiener-Hopf Eq. (C-7) can be rewritten as:

$$\frac{2}{\sqrt{k_o-k}}\,\frac{\partial \bar{\bar{\phi}}_{1+}}{\partial y} = \imath\sqrt{k_o+k}\left(\bar{\bar{\phi}}_{1-} - \bar{\bar{\phi}}_{2-}\right) - \frac{e^{-\imath(kx_o+\gamma_1 y_o)}}{4\pi^2 a^2\sqrt{k_o-k}} . \tag{C-10}$$

The last term of Eq. (C-10) can be decomposed into the sum of plus and minus functions as:

$$F_1(k) = \frac{e^{-i(kx_o+\gamma_1 y_o)}}{4\pi^2 a^2 \sqrt{k_o-k}} = F_{1+}(k) + F_{1-}(k) \quad , \tag{C-11a}$$

where F_{1+}, F_{1-} are given as:

$$\left.\begin{aligned} F_{1+}(k) &= \frac{-1}{2\pi i} \int_{C+} \frac{F(\lambda)}{\lambda-k}\, d\lambda \\ F_{1-}(k) &= \frac{1}{2\pi i} \int_{C-} \frac{F(\lambda)}{\lambda-k}\, d\lambda \quad . \end{aligned}\right\} \tag{C-11b}$$

The contours C_+ and C_- lie in the common region (C-8) and C_+ passes above $\lambda = k$ and C_- passes below $\lambda = k$. The exponential decays of $F(\lambda)$ on the contour, since $\mathrm{Im}\gamma_1 > 0$, $y_o < 0$, ensures that these integral exist and that $F_{1+}(k) = 0\left(|k|^{-1}\right)$, $F_{1-}(k) = 0\left(|k|^{-1}\right)$ as $k \to \infty$ in respective regions.

The Wiener-Hopf equation now takes the form as:

$$\frac{2}{\sqrt{k_o - k}} \frac{\partial \bar{\bar{\phi}}_{1+}}{\partial y} + F_{1+} = i\sqrt{k_o + k}\left(\bar{\bar{\phi}}_{1-} - \bar{\bar{\phi}}_{2-}\right) - F_{1-} = C(k) \quad . \tag{C-12}$$

The function $C(k)$ is the entire function of k and must be a regular function of k in the whole k-plane. At the plate edge, we assume:

$$\frac{\partial \bar{\phi}_{1+}}{\partial y} \to O\left(x^{-1/2}\right) \qquad \text{as} \quad x \to +0 \quad \text{on} \quad y = +0 \tag{C-13a}$$

$$\bar{\phi}_1 \to C_1(\omega) \qquad \text{as} \quad x \to -0 \quad \text{on} \quad y = +0 \tag{C-13b}$$

$$\bar{\phi}_2 \to C_2(\omega) \qquad \text{as} \quad x \to -0 \quad \text{on} \quad y = -0 \,. \tag{C-13c}$$

Carrying out the half-range Fourier transform defined by Eq. (2-7), the asymptotic behavior of the above functions can be calculated with the aid of the Abelian theorem as:

$$\frac{\partial \bar{\bar{\phi}}_{1+}}{\partial y} = O\left(|k|^{-1/2}\right) \qquad \text{as} \quad k \to \infty \quad \text{in} \quad \text{Im}k < \text{Im}k_o \tag{C-14a}$$

$$\bar{\bar{\phi}}_{1-} = O\left(|k|^{-1}\right) \qquad \text{as} \quad k \to \infty \quad \text{in} \quad \text{Im}k > -\text{Im}k_o \tag{C-14b}$$

$$\bar{\bar{\phi}}_{2-} = O\left(|k|^{-1}\right) \qquad \text{as} \quad k \to \infty \quad \text{in} \quad \text{Im}k > -\text{Im}k_o \,. \tag{C-14c}$$

Hence from Eq. (C-12)

$$C(k) = O\left(|k|^{-1}\right) \qquad \text{as} \quad k \to \infty \quad \text{in} \quad \text{Im}k < \text{Im}k_o \tag{C-15a}$$

$$C(k) = O\left(|k|^{-1/2}\right) \qquad \text{as} \quad k \to \infty \quad \text{in} \quad \text{Im}k > -\text{Im}k_o \,. \tag{C-15b}$$

C(k) is regular in the whole k-plane and tends to zero as k tends to infinity in any direction. Hence from Liouville's theorem C(k) must be identically zero. Therefore, we obtain:

$$\frac{\partial \bar{\bar{\phi}}_{1+}}{\partial y} = \frac{-\sqrt{k_o - k}\, F_{1+}(k)}{2} \,, \tag{C-16}$$

$$A_1(k,\omega) = \bar{\bar{\phi}}_1 \Big|_{y=0}$$

$$= \frac{1}{i\gamma_1} \frac{\partial \bar{\bar{\phi}}_1}{\partial y}$$

$$= \frac{-i}{\gamma_1} \frac{\partial \bar{\bar{\phi}}_{1+}}{\partial y}$$

$$= \frac{iF_{1+}(k)}{2\sqrt{k_o + k}} \,. \qquad \text{(C-17)}$$

APPENDIX D

THE SOLUTION FOR THE INFINITE VORTEX SHEET PROBLEM

The governing differential equations are the same as Eq. (2-1). The boundary conditions (2-4), (2-5a), and (2-5b) must be satisfied throughout the vortex sheet. Instead of the half-range Fourier transform, using the full-range transform, Eqs. (2-4), (2-5a), and (2-5b) can be written as:

$$\alpha\bar{\bar{\phi}}_2 = \bar{\bar{\phi}}_1 \tag{D-1}$$

$$\frac{\partial\bar{\bar{\phi}}_2}{\partial y} = -\imath\omega\alpha\bar{\bar{h}} \tag{D-2}$$

$$\frac{\partial\bar{\bar{\phi}}_1}{\partial y} = -i\omega\bar{\bar{h}} \ . \tag{D-3}$$

From Eqs. (D-2) and (D-3) we obtain:

$$\alpha\,\frac{\partial\bar{\bar{\phi}}_1}{\partial y} = \frac{\partial\bar{\bar{\phi}}_2}{\partial y} \ . \tag{D-4}$$

From Eq. (2-12)

$$\bar{\bar{\phi}}_1\Big|_{y=0} = A_1$$

$$\bar{\bar{\phi}}_2\Big|_{y=0} = A_2 + \frac{e^{-\imath kx_o}\sin\gamma_2 y_o}{4\pi^2 a^2 \gamma_2}$$

$$\left.\frac{\partial\bar{\bar{\phi}}_1}{\partial y}\right|_{y=0}$$

$$\left.\frac{\partial\bar{\bar{\phi}}_2}{\partial y}\right|_{y=0} = -\imath\gamma_2 A_2 - \frac{e^{-ikx_o}\cos\gamma_2 y_o}{4\pi^2 a^2} \,. \tag{D-5}$$

Substituting Eq. (D-5) into Eqs. (D-1) and (D-4) gives

$$\left.\begin{aligned} \alpha A_2 + \frac{\alpha\, e^{-ikx_o}\sin\gamma_2 y_o}{4\pi^2 a^2 \gamma_2} &= A_1 \\ \imath\alpha\gamma_1 A_1 &= -\imath\gamma_2 A_2 - \frac{e^{-ikx_o}\cos\gamma_2 y_o}{4\pi^2 a^2} \,. \end{aligned}\right\} \tag{D-6}$$

Finally, from Eq. (D-6), A_1 and A_2 are determined as:

$$\left.\begin{aligned} A_1 &= \frac{\imath\alpha\, e^{-\imath kx_o - i\gamma_2 y_o}}{4\pi^2 a^2 (\gamma_2 + \alpha^2\gamma_1)} \\ A_2 &= \frac{i\, e^{-ikx_o}}{8\pi^2 a^2 \gamma_2} \left(e^{i\gamma_2 y_o} + \frac{\gamma_2 - \alpha^2\gamma_1}{\gamma_2 + \alpha^2\gamma_1} e^{-i\gamma_2 y_o} \right) \,. \end{aligned}\right\} \tag{D-7}$$

REFERENCES

1. Jones, D.S., and Morgan, J.D., "The Instability of a Vortex Sheet on a Subsonic Stream Under Acoustic Radiation," Proc. Camb. Phil. Soc., 72, 1972, pp. 465-488.

2. Jones, D.S., "The Reflexion of an Acoustic Pulse by a Plane Vortex Sheet," Proc. Camb. Phil. Soc., 74, 1973, pp. 349-364.

3. Jones, D.S., "The Instability Due to an Acoustic Radiation Striking a Vortex Sheet on a Supersonic Stream," Proc. R.S.E. (A), 71, 11, 1972-1973, pp. 121-140.

4. Hardisty, N., "The Instability Due to an Acoustic Radiation Striking a Vortex Sheet on a Supersonic Stream," Proc. R.S.E. (A), 71, 12, 1972-1973, pp. 141-149.

5. Hardisty, N., "The Instability of Two Vortex Sheets Enclosing a Subsonic Jet Due to an Acoustic Point Source," Proc. R.S.E. (A), 73, 13, 1974-1975, pp. 215-229.

6. Chao, C.C., "Transmitted Sound Field Due to an Impulsive Line or Point Acoustic Source Through a Plane Vortex Sheet," to appear.

7. Carrier, G., Krook, M., and Pearson, C., "Functions of a Complex Variable," McGraw-Hill, 1966.

8. Noble, B., "Method Based on the Wiener-Hopf Technique," London, Pergamon, 1958.

9. Orszag, S.A., and Crow, S.C., "Instability of a Vortex Sheet Leaving a Semi-Infinite Plate," Studies in Appl. Math., XLIX 2, 1970, pp. 167-181.

10. Crighton, D.C., "Radiation Properties of the Semi-Infinite Vortex Sheet," Proc. R. Soc. A 330, 1972, p. 185.

11. Morgan, J.D., "The Interaction of Sound with a Semi-Infinite Vortex Sheet," Quart. J. Mech. Appl. Math., 27, 1974, pp. 465-487.

12. Crighton, D.C., and Leppington, F.G., "Radiation Properties of the Semi-Infinite Vortex Sheet: The Initial-Value Problem," J. Fluid Mech., 64, 1974, pp. 393-414.

13. Jones, D.S., and Morgan, J.D., "A Linear Model of a Finite Amplitude Helmholtz Instability," Proc. R. Soc. A 338, 1974, pp. 17-41.

14. Morgan, J.D., "The Interaction of Sound with a Subsonic Cylindrical Vortex Sheet," Proc. R. Soc. A 344, 1975, pp. 341-362.

15. Munt, R.M., "The Interaction of Sound with a Subsonic Jet Issuing from a Semi-Infinite Cylindrical Pipe," J. Fluid Mech., 83, 1977, pp. 609-640.

16. Howe, M.S., "The Influence of Vortex Shedding on the Generation of Sound by Convected Turbulence," J. Fluid Mech., 76, 1976, pp. 711-740.

17. Daniels, P.G., "Viscous Mixing at the Trailing Edge," Quart. J. Appl. Math., 30, 1977, pp. 319-342.

18. Bechert, D., and Pfizenmaier, E., "Optical Compensation Measurements on the Unsteady Exit Condition at the Nozzle Discharge Edge," J. Fluid Mech., 71, 1975, pp. 123-144.

End of Document